Progress in Oceanography 191 (2021) 102497

Contents lists available at ScienceDirect

Progress in Oceanography

journal homepage: www.elsevier.com/locate/pocean

Benthic hotspots on the northern Bering and Chukchi continental shelf: Spatial variability in production regimes and environmental drivers

Zhixuan Feng [a,b,c,*], Rubao Ji [b], Carin Ashjian [b], Jinlun Zhang [d], Robert Campbell [e], Jacqueline M. Grebmeier [f]

[a] State Key Laboratory of Estuarine and Coastal Research, School of Marine Sciences, and Institute of Eco-Chongming (IEC), East China Normal University, Shanghai, China
[b] Department of Biology, Woods Hole Oceanographic Institution, Woods Hole, MA, USA
[c] Southern Marine Science and Engineering Guangdong Laboratory (Zhuhai), Zhuhai, China
[d] Applied Physics Laboratory, University of Washington, Seattle, WA, USA
[e] Graduate School of Oceanography, University of Rhode Island, Narragansett, RI, USA
[f] Chesapeake Biological Laboratory, University of Maryland Center for Environmental Science, Solomons, MD, USA

ARTICLE INFO

Keywords:
Polar marine ecosystem
Benthic biological hotspots
Pelagic-benthic coupling
Ice-ocean-biogeochemical model
Particle tracking model
Bering and Chukchi seas

ABSTRACT

Benthic biological hotspots with persistently high macrofaunal biomass exist on the highly advective continental shelf that extends from the northern Bering Sea to the northeast Chukchi Sea. Environmental factors that influence carbon export to the benthos, a key driver for hotspot formation and persistence, remain uncertain. Multiple modeling approaches were used to better understand the combined effects of biological production and physical transport processes on supplying biogenic materials to those biological hotspots. Large data sets of benthic and environmental observations were synthesized, outputs from a pan-arctic ice-ocean-biogeochemical model were analyzed, and particle tracking modeling experiments and statistical analyses were conducted. Two different biophysical mechanisms of biogenic material supply to five benthic hotspot subdomains over a latitudinal range were identified using models and verified using data synthesis. Two hotpots to the south and the north of Bering Strait and the third one in southern Barrow Canyon heavily rely on carbon supplied from upstream biological production. In contrast, the St. Lawrence Island Polynya, southwest of St. Lawrence Island in the northern Bering Sea, and the Northeast Chukchi Sea hotspots are mostly fueled by local production. Spatial statistical modeling of benthic biomass distribution generally recaptured known hotspots but also suggested the likelihood of other probable hotspots in subregions of the biologically productive Gulf of Anadyr and of the topographically controlled Herald Canyon where limited sampling has occurred. The study provides new mechanistic understandings of the oceanographic processes and biophysical interactions that produce organic matter in sea ice and in the water column that subsequently is exported to underlying benthic communities. Combining data synthesis with process-based modeling was critical in understanding the dynamics of these sympagic-pelagic-benthic ecosystems and the potential climate-change-induced ecosystem response in the Pacific Arctic region.

1. Introduction

The northern Bering Sea and the Chukchi Sea contain a wide continental shelf with a unique polar marine ecosystem that is biologically productive but greatly influenced by seasonal sea ice cover and northward-flowing Pacific water masses, nutrients, organic materials, and marine organisms (Walsh et al., 1989; Springer et al., 1996). This region is the only gateway for the Pacific water that enters the interior Arctic with an annual climatological mean transport of approximately 0.8 Sv (1 Sv = 10^6 m^3 s^{-1}) through Bering Strait (Coachman and Aagaard, 1988; Woodgate, 2018). Decades of research have made substantial progress in understanding this advective shelf ecosystem, and its responses and feedbacks to the whole Arctic system (see reviews of Grebmeier, 2012; Dunton et al., 2014; Grebmeier et al., 2015a). Five benthic hotspot subdomains exist in the northern Bering and Chukchi continental shelf (see Fig. 1 bounding boxes). From south to north, the

* Corresponding author at: 500 Dongchuan Road, A305 Estuarine and Coastal Building, East China Normal University, Shanghai 200241, China.
E-mail address: zxfeng@sklec.ecnu.edu.cn (Z. Feng).

https://doi.org/10.1016/j.pocean.2020.102497
Received 14 June 2019; Received in revised form 4 October 2020; Accepted 7 December 2020
Available online 11 December 2020

five subdomains are the St. Lawrence Island Polynya (SLIP), Chirikov Basin in the Northern Bering Sea (Chirikov), Southern Chukchi Sea (SCS), Northeastern Chukchi Sea (NECS), and Barrow Canyon (BC) (Grebmeier et al., 2006a; Grebmeier, 2012; Grebmeier et al., 2015a). Since 2010, those regions have been annually sampled by the international Distributed Biological Observatory (DBO) program, a network of fixed stations and transects for detecting concurrent physical and biological changes (Moore and Grebmeier, 2018).

The interplay among water mass transport, sea ice dynamics, nutrient availability, ice algal and pelagic primary production, zooplankton grazing, transformation of organic materials in the water column, seafloor habitat features, and benthic processes likely determine the spatial distribution and species composition of benthic biomass hotspots (Grebmeier et al., 2015a). Benthic communities serve as long-term integrators of exported organic materials that sink, accumulate, and decompose in the underlying sediment, and the biomass and community composition of the benthic organisms can help infer physical-biological processes in the overlying water column (Pirtle-Levy et al., 2009; Iken et al., 2010). Benthic bulk parameters, such as macroinfaunal carbon biomass and sediment community oxygen consumption, have been widely used in exploring ecological responses of the benthos to environmental drivers in the Pacific Arctic region (e.g., Dunton et al., 2005; Grebmeier, 2012; Grebmeier et al., 2015b; Lovvorn et al., 2016). For instance, to assess ecosystem-forcing factors that form and maintain four benthic hotspot subdomains in the northern Bering and Chukchi seas (not including the Barrow Canyon subdomain), Grebmeier et al. (2015a) synthesized extensive ocean environmental measurements (such as sea ice, temperature, salinity, currents, and nutrients) and biological sampling datasets (chlorophyll-a in sea ice and water column, benthic macrofaunal abundance, biomass, and species composition, demersal fish abundance, biomass, and species richness, and benthic-foraging seabirds and mammals). That review depicted distinctive characteristic patterns of the four benthic hotspots and highlighted that bottom-up forcing by hydrography and food supply largely affected hotpot formation and persistence (Grebmeier et al., 2015a). However, knowledge gaps still exist regarding food supply mechanisms for those hotspots and their relationships with hydrographic forcing. For example, how do nutrient supply, primary production, and physical transport processes co-work to produce and deliver biogenic materials from the ice and water column to the seafloor? The development of dynamically coupled physical-biogeochemical models that complement historical and ongoing field programs will facilitate a system-level and

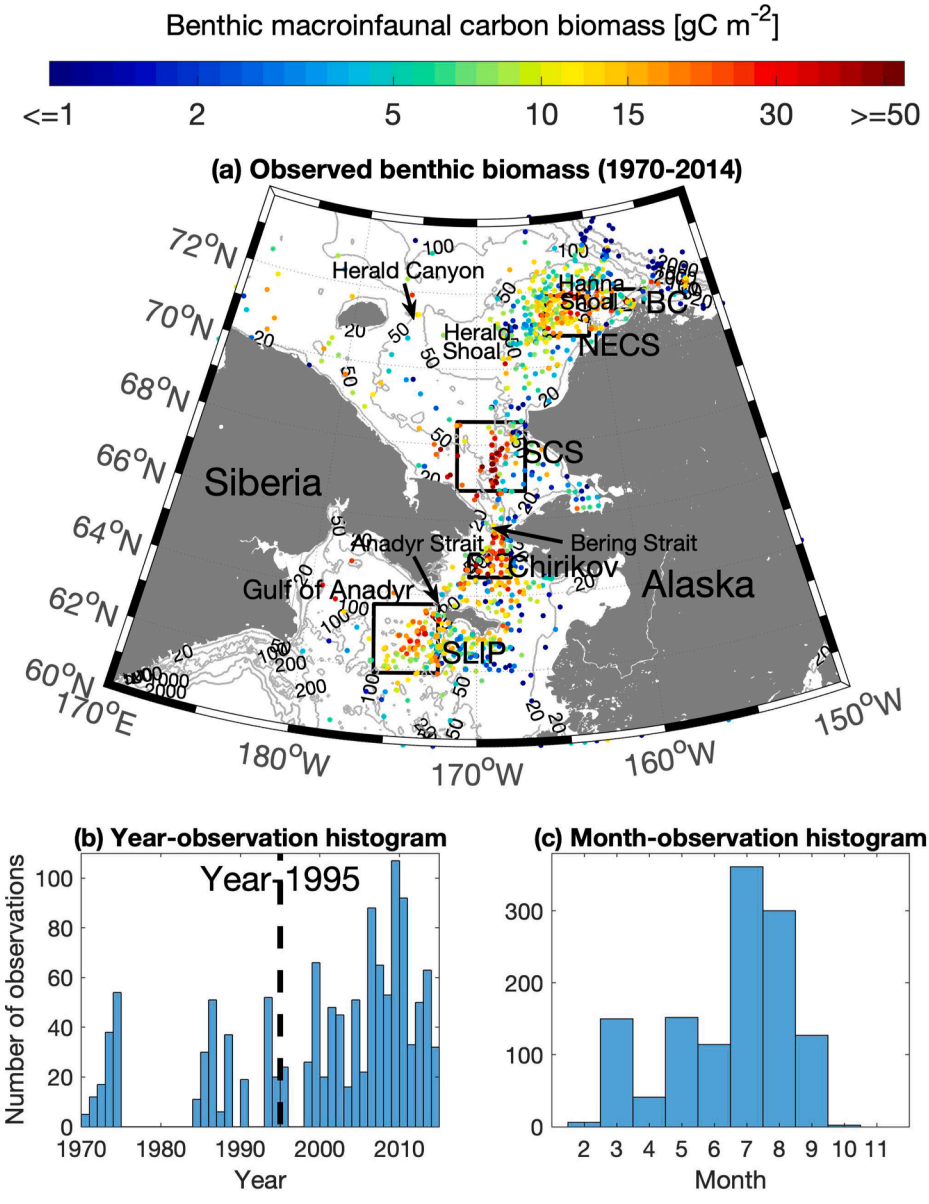

Fig. 1. Distribution of benthic biomass observations (1970–2014) and benthic hotspot bounding boxes in the northern Bering and Chukchi Seas. (a) Observed benthic biomasses from 1970 to 2014, (b) histogram of observations through years, and (c) histogram of observations through months. The scattered dots represent sampling locations and the colors illustrate benthic macroinfaunal carbon biomass (dry weight) per square meter (g C m^{-2}) on a logarithmic scale. Isobaths of 20, 50, 100, 200, 1000, and 2000 m are superimposed. Solid line bounding boxes depict geographic domains of 5 hotspot subdomains from southwest to northeast: St. Lawrence Island Polynya (SLIP), Chirikov Basin in the Northern Bering Sea (Chirikov), South Chukchi Sea (SCS) north of Bering Strait, Northeast Chukchi Sea (NECS), and Barrow Canyon (BC).

mechanistic understanding of this productive but potentially vulnerable polar marine ecosystem.

The present study applied data analysis and modeling approaches to better understand the interplay between biological production and physical transport processes on supplying biogenic materials to various hotspot subdomains in the northern Bering and Chukchi seas. First, the spatial distribution of benthic macroinfaunal biomass was described by analyzing a large data set of historical benthic sampling. Then, a pan-arctic ice-ocean-biogeochemical model forced by realistic atmospheric, oceanic, and biogeochemical conditions was run to diagnose the standing stocks of multiple biological variables and to evaluate physical and biological contributions to the particulate organic matter pool. Backward-in-time Lagrangian particle tracking experiments were conducted to quantify spatiotemporal scales of biogenic particles that initially settle to the seafloor. Lastly, model results were incorporated into a statistical framework to reconstruct the spatial distribution of benthic macrofaunal biomass and to also indicate the location of potential hotspots in data-limited regions. Combining data synthesis with process-based and statistical modeling greatly improved our understandings of the distinctive driving mechanisms in food supply to different benthic hotspots along the latitudinal gradient from the northern Bering Sea to the northeast Chukchi Sea. Mechanistic understandings of the biophysical interactions are essential to disentangle different processes in forming and maintaining those hotspots and to further predict future ecosystem reorganization in the rapidly changing Pacific Arctic region.

2. Data and methods

2.1. Data compilation and processing

Benthic biomass distributions were compiled from multiple synthesis data products over a 4-decade period (1970–2014). Satellite-retrieved chlorophyll-a and mooring hydrographic data also were assembled to validate the ice-ocean-biogeochemical model. To evaluate the benthic datasets under a standardized spatial framework, a grid mesh of 0.5 longitudinal degrees (16–28 km) and 0.25 latitudinal degrees (~28 km) within the geographic domain of 170°E-150°W and 60°N-74°N was created. Bottom depths at the centers of the mesh were interpolated from NOAA's ETOPO1 1 arc-minute Global Relief Model (Amante and Eakins, 2009). Depths that were shallower than 20 m or deeper than 200 m were masked.

2.1.1. Benthic macroinfaunal data

The benthic biological and sediment data were originally synthesized by the Pacific Marine Arctic Regional Synthesis (PacMARS), which comprised shipboard sampling from multiple research cruises since the 1970s (Grebmeier and Cooper, 2014; Grebmeier et al., 2015a; 2015b). For this study, benthic macroinfaunal dry weight carbon biomass was used to depict the spatial distribution of benthic biomass (regardless of species composition and biodiversity) and to infer benthic biological hotspots. Because PacMARS only synthesized cruise data until 2012, additional data in 2013 and 2014 archived in the Arctic Data Center (https://arcticdata.io) were supplemented to the PacMARS data (Grebmeier and Cooper, 2018a; 2018b). Available benthic biomass observations were highly heterogeneous in space with much better data coverage in the US Alaskan side than in the Russia Siberian side (Fig. 1a). To analyze together with the available satellite and model data, benthic observational data collected during two recent decades (1995–2014; $n = 901$) were retained, which included 72% of all available data points in the domain of interest (Fig. 1b). Also, the majority of the field cruises occurred in the late spring to early fall seasons with the summer months of July and August being the most frequent (Fig. 1c).

2.1.2. Satellite ocean color data

Satellite-derived 8-day composite 0.25° (~25 km) chlorophyll-a concentrations (1998–2014) were downloaded from the GlobColour data server (http://hermes.acri.fr). The GlobColour product utilized a semi-analytical Garver-Siegel-Maritorena (GSM) method to merge the normalized water-leaving reflectance in the sensor wavelengths from multiple ocean color satellite missions (SeaWiFS, MODIS, MERIS, and VIIRS) and to further generate a global coverage of chlorophyll-a concentrations (Maritorena and Sigel, 2005; Maritorena et al., 2010). This chlorophyll-a concentration (mg m^{-3}) represents case-1 waters (CHL1) where the phytoplankton concentration dominates inorganic particles. Not all Bering and Chukchi waters were case-1 waters due to the presence of suspended sediment and/or color dissolved organic matter (CDOM). To partially resolve this issue, the coastal regions shallower than 20 m were masked. April-September values in the Bering-Chukchi domain were averaged to construct a spring-summer mean sea surface chlorophyll-a climatology. Because of cloudiness, ice coverage, and polar night conditions, ocean color data from October to March (fall and winter) are very sparse, especially in the northernmost latitudes adjacent to the Arctic basins.

2.1.3. Mooring hydrographic data

The 20-year (1995–2014) annual mean water volume, heat, and freshwater fluxes through Bering Strait were retrieved from a data repository at the University of Washington Polar Science Center (http://psc.apl.washington.edu/BeringStrait.html). Those annual fluxes were calculated from long-term mooring observations (see Woodgate et al., 2015; Woodgate, 2018 for details) and were used to validate model-derived annual transport.

2.2. Ice-ocean-biogeochemical model

Physical and biological processes were diagnosed and analyzed using a pan-arctic ice-ocean-biogeochemical coupled model, namely the Biology-Ice-Ocean Modeling and Assimilation System (BIOMAS; Zhang et al., 2010). This model resolves the seasonality and interannual variability of the ocean physics and biology, including general ocean circulation, sea ice and snow, biogeochemical cycling, and primary and secondary productions in the water column. BIOMAS has also been used for previous community-based ecosystem model intercomparison studies (Popova et al., 2012; Jin et al., 2016; Lee et al., 2016).

The pan-arctic model domain covers the entire North Hemisphere northward of 39°N (Fig. 2a). Its generalized orthogonal curvilinear mesh places the "north pole" in the center of Alaska to eliminate the singularity issue at the geographic North Pole (Zhang et al., 2015). This grid configuration also leads to much finer horizontal resolutions in the Pacific Arctic than the Atlantic Arctic (~4 km in the Bering Strait versus ~ 100 km in the Barents Sea; Zhang et al., 2015). The model can be regarded as eddy-permitting in the Pacific Arctic, as the mean horizontal resolution (~10 km) approximates the Rossby radius of deformation of ~ 9 km (Nurser and Bacon, 2014) and the model has 40 layers of varying thicknesses in a Z-coordinate. The upper 80 m contains 16 layers of 5 m each, and the upper 120 m has 21 layers in total. High resolution in the upper water column is conducive for resolving processes in the shallow continental shelf, surface mixed layer, and upper euphotic zone.

BIOMAS includes dynamically coupled sub-models for sea ice and snow, ocean circulation, and biogeochemical cycling in both ocean and ice. NOAA's Climate Forecast System (CFS) reanalysis data (Saha et al., 2010) are downscaled and interpolated to the model grid as atmospheric forcing. The physical model for the ice and ocean is based on the Marginal Ice Zone Modeling and Assimilation System (MIZMAS, Schweiger and Zhang, 2015; Zhang et al., 2016), which is the latest version of the Pan-arctic Ice-Ocean Modeling and Assimilation System (PIOMAS, Zhang and Rothrock, 2003). The model assimilates sea ice concentration in ice-covered areas following Lindsay and Zhang (2006) and sea surface temperature (SST) in open water areas following Manda et al. (2005). The ice concentration and SST data were obtained from the National Snow and Ice Data Center and CFS reanalysis products, respectively.

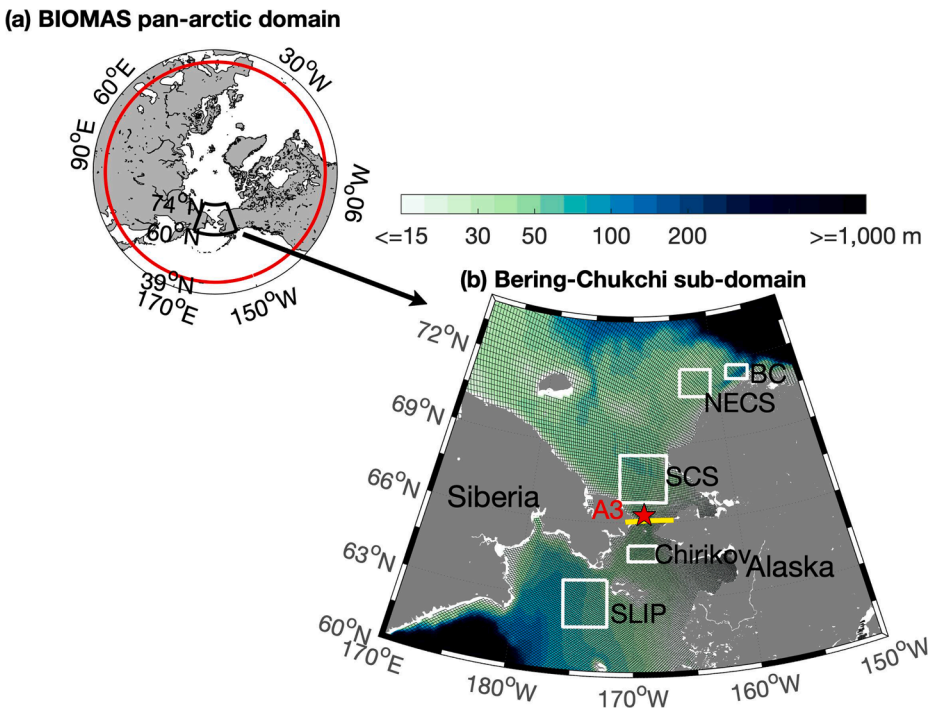

Fig. 2. The entire domain of the ice-ocean-biogeochemical model Biology-Ice-Ocean Modeling and Assimilation System (BIOMAS), and its high spatial resolution subdomain in the northern Bering and Chukchi Seas. (a) Pan-arctic model domain and its open boundary. (b) Subdomain of interest in the northern Bering and Chukchi Seas of the Pacific Arctic. In Panel (a), the red circle represents the model's open boundary at 39°N. In Panel (b), the red star illustrates A3 mooring (~35 km north of Bering Strait) that is used to validate the BIOMAS-derived Bering Strait transect (yellow line) throughflow, background colors illustrate model bathymetry, and white bounding boxes represent the five benthic biological hotspot subdomains. (For interpretation of the references to color in this figure legend, the reader is referred to the web version of this article.)

This model version also allows for melt pond distribution (Zhang et al., 2018). For model-observation synthesis studies using extensive ice, snow, hydrographic and biogeochemical measurements, refer to Zhang et al. (2010, 2014, 2015, 2016, and 2018).

The lower-trophic-level biogeochemical model is adapted to the Arctic Ocean based on the North Pacific Ecosystem Model for Understanding Regional Oceanography (NEMURO; Kishi et al., 2007). This nitrogen-based biogeochemical model includes two phytoplankton components (diatoms and flagellates), three zooplankton components (microzooplankton, mesozooplankton, and predator zooplankton), dissolved organic nitrogen (DON), particulate organic nitrogen (PON), particulate organic silica (Opal), nitrate (NO_3), ammonium (NH_4), and silicate (Fig. 3). The sea ice algae model has two ice algal components representing diatoms and flagellates, with nitrate, ammonium, and silicate as limiting nutrients for algal growth within the bottom 2 cm sea ice skeletal layer (Jin et al., 2006). Modeled ice algal biomass concentrations compared well with ice core stations on the shelf and slope regions of the Chukchi and Beaufort seas during the Shelf-Basin Interaction (SBI) studies (Gradinger, 2009). Note that BIOMAS doesn't distinguish between ice algal and pelagic phytoplankton species, so the

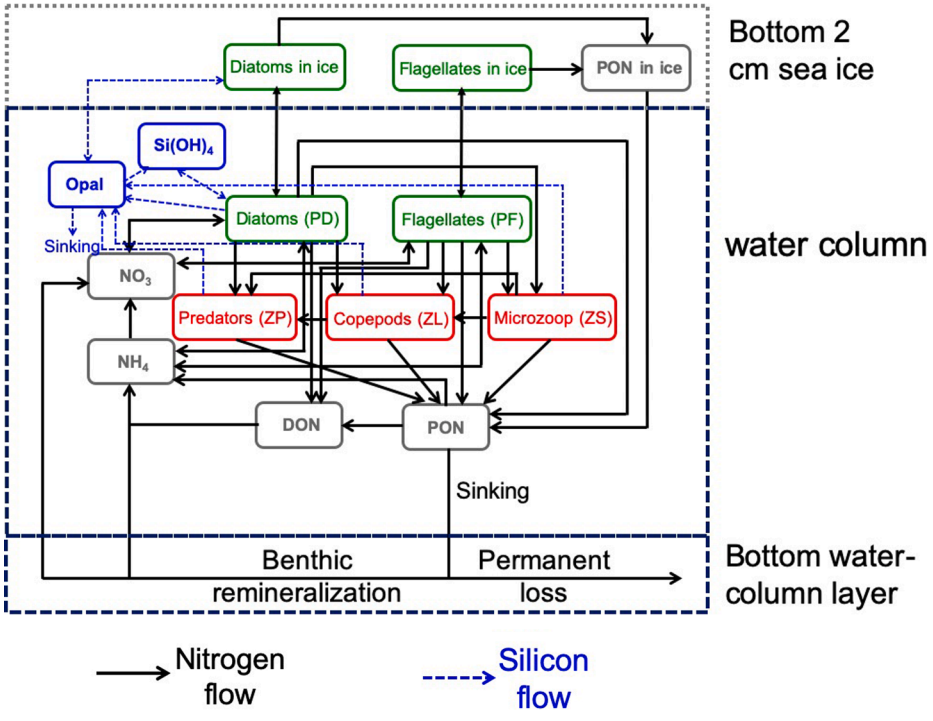

Fig. 3. BIOMAS biogeochemical model structure for the ice and pelagic ecosystem. The upper box represents the bottom 2-cm sea ice layer for simulating ice algal growth. The lower box represents the entire water column and the bottom water-column layer is singled out for benthic feedback processes in the bottom boundary layer, i.e., fixed proportions of sinking PON being remineralized (benthic remineralization) and removed (permanent burial or outgas). For simplicity, nutrient (NO_3 and NH_4) components in the ice layer are omitted.

two ice algal components join their water column counterparts once the sea ice melts. Also, a constant sinking velocity of 20 m d^{-1} for PON and Opal is specified while other model components do not sink vertically. Additionally, the model itself does not have a benthic/sediment biogeochemical model; instead, it implements simple benthic feedback mechanisms in the bottom water-column layer to mimic benthic remineralization and loss (burial or denitrification) processes, similar to Fennel et al. (2006). The remineralization of deposited organic matter in the upper part of the sediment is formulated as a bottom boundary condition. Essentially, the flux of sinking particulate organic matter out of the bottommost grid box results immediately in a corresponding influx of inorganic nutrients at the water–sediment interface. This approach, of intermediate complexity in a hierarchy of benthic-pelagic coupling formulations, has proven to be effective in representing the nitrogen cycling processes in the water column and organic matter remineralization at the water–sediment interface that explicitly accounts for sediment denitrification (Soetaert et al., 2000; Fennel et al., 2006). The benthic remineralization is represented by immediately converting 2.5% of the sinking PON flux to the nitrate pool and the other 2.5% to the ammonium pool (i.e., instantaneous consumptions of sinking materials by benthic fauna). The loss processes are quantified by immediate removal of 5% of the sinking PON flux in the bottom water-column layer. The above percentages were estimated to match the orders of magnitude of sedimentary denitrification rates previously reported in the region (Devol et al., 1997). The remaining 90% of sinking PON accumulates in the bottom water column layer and slowly decomposes to DON and NH_4 (i.e., temperature-dependent slow decomposition of settled organic matter by both benthic fauna and water-column processes; see Fig. 3).

The daily mean BIOMAS outputs from 1995 to 2014 were utilized in the following five analyses:

(1) Daily mean fluxes of water volume, heat, and freshwater through Bering Strait were integrated through a corresponding model transect (see Fig. 2b yellow line) in each of the calendar years, and further compared with mooring-derived transport (see Section 2.1.3). When calculating heat and freshwater fluxes, we followed Woodgate et al. (2015) and Woodgate (2018) by referencing to a freezing temperature (−1.9 °C) and mean Arctic seawater salinity (34.8 PSU). Note that the mooring-based transport calculation assumed homogenous water properties across the Bering Strait with a cross-sectional area of 4.25 km^2 and extrapolated A3 mooring observations to the whole Bering Strait (Woodgate, 2018). In contrast, the model-based transport calculation integrated fluxes across the Strait with a cross-sectional area of 3.46 km^2. The methodological differences in flux calculations may result in some discrepancies in observed versus modeled fluxes (see Section 3.2).
(2) The 20-year climatological mean ice algal, phytoplankton, and PON standing stocks were diagnosed for the spatial distribution of long-term inventories of potential food production and supplies for the benthos.
(3) Model results were used to separate biological versus physical contributions to the particulate organic matter (POM) pool (see Section 2.3).
(4) BIOMAS daily velocity fields served as physical forcing for tracking sources and pathways of biogenic particles that initially settle to the seafloor (see Section 2.4).
(5) Physical and biological parameters were bilinearly interpolated to the standardized mesh for conducting statistical analysis (see Section 2.5).

2.3. Diagnostic analysis of biological and physical contributions to the POM pool

The biological and physical effects on the POM pool, including phytoplankton (representing live microalgae) and PON (representing only detritus), was separated by using 2-dimensional depth-integrated mass balance equations for total water column phytoplankton (PT) that include planktonic flagellates (PF) and diatoms (PD), and PON (see Fig. 4). All variables are expressed in nitrogen units because the biogeochemical model is nitrogen-based.

$$\int_0^H \frac{\partial PT}{\partial t} = \int_0^H PT_{Phy} + \int_0^H PT_{Bio} + PT_{Ice2Wtr}$$

$$\int_0^H \frac{\partial PON}{\partial t} = \int_0^H PON_{Phy} + \int_0^H PON_{Bio} + PON_{Ice2Wtr} - SED_{PON}$$

where the left-hand side terms represent temporal changes of whole water column PT or PON stocks (i.e., time derivatives of depth-integrated PT or PON concentrations), the right-hand sides have physical and biological rates of change terms and interfacial flux terms, and H is the total water depth. $PT_{Ice2Wtr}$ is the ice-water phytoplankton exchange flux, $PON_{Ice2Wtr}$ is the ice-water PON exchange flux, and SED_{PON} is the PON sedimentation loss rate.

The depth-integrated net biological rate of change for PT was directly calculated as:

$$\int_0^H PT_{Bio}dz = \int_0^H (Gpp_{PT} - Res_{PT} - Mor_{PT} - Exc_{PT} - Gra_{P2Z})dz$$

where right-hand terms are gross primary productivity, phytoplankton respiration, mortality, excretion, and grazing by three zooplankton groups, respectively. All those biological rate terms can be outputted directly from the biogeochemical model.

The depth-integrated net biological rate of change for PON was expressed as:

$$\int_0^H PON_{Bio}dz = \int_0^H (Mor_{PT} + Mor_Z + Ege_Z - Dec_{PON})dz$$

where right-hand terms are phytoplankton mortality, zooplankton mortality, zooplankton egestion, and PON decomposition, respectively.

Finally, the physical contributions to the mass balance were represented by the residual rates of change:

$$\int_0^H PT_{Phy}dz = \int_0^H \frac{\partial PT}{\partial t}dz - \int_0^H PT_{Bio}dz - PT_{Ice2Wtr}$$

$$\int_0^H PON_{Phy}dz = \int_0^H \frac{\partial PON}{\partial t}dz - \int_0^H PON_{Bio}dz - PON_{Ice2Wtr} + SED_{PON}$$

2.4. Lagrangian particle tracking model

A Lagrangian particle tracking model was used to determine the advective spatiotemporal scales and source regions of biogenic particles that ultimately settle to the hotspots (see Fig. 5 schematic diagram). This model was modified from an existing individual-based model that was coupled offline to BIOMAS (Feng et al., 2016; 2018). In principle, it numerically solves an advection equation based on a high-accuracy 4th-order Runge-Kutta (RK4) method. The particle velocities at instantaneous time and location were linearly interpolated from the 3-D daily mean flow fields. To mimic the descending nature of biogenic particles across the size spectrum from μm to mm, various vertical sinking speeds from 1 (e.g., tiny phytoplankton cells) to 50 (e.g., marine snow aggregates) meters per day (m d^{-1}) were assigned to virtual particles, assuming biogenic particles do not change their sinking velocities (or sizes) in the water column. The 1 m d^{-1} for planktonic cells corresponded to both laboratory experiments and analytical models (Miklasz and Denny, 2010), and the 50 and 100 m d^{-1} for marine snow was based on video plankton record measurements in the northeast Chukchi Sea (Ashjian et al., 2005). All particles were initially located on the seafloor and inversely tracked in time until they reversed back to the sea surface

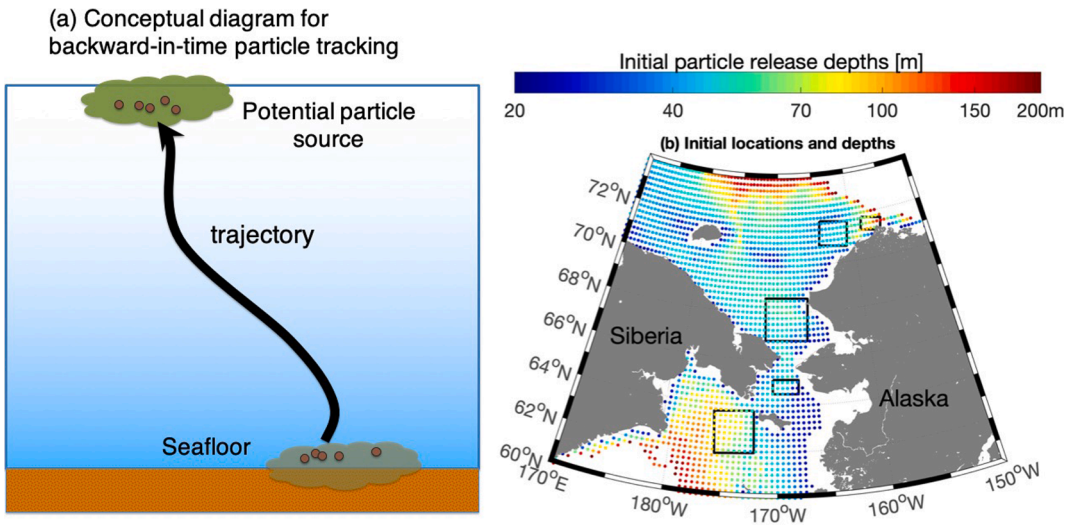

Fig. 4. Backward-in-time Lagrangian particle tracking experiments. (a) A conceptual diagram illustrating seafloor-settled particles that are backtracked to the sea surface where biogenic particles are produced. (b) Initial horizontal locations and depths of tracked particles (corresponding seafloor depths) in the domain of the northern Bering and Chukchi Seas.

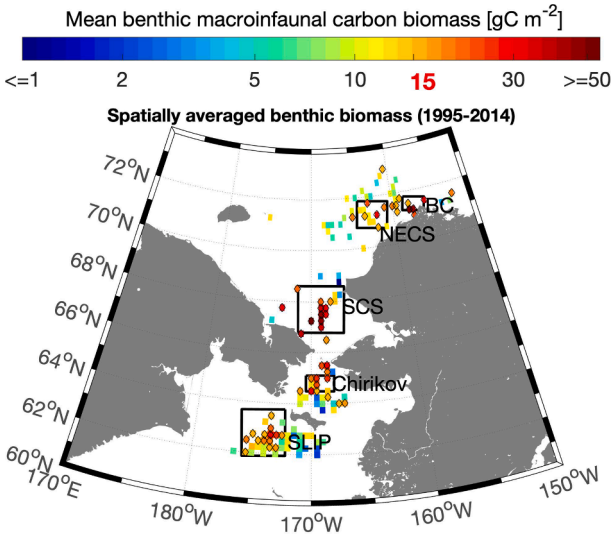

Fig. 5. Spatially averaged benthic macroinfaunal carbon biomass (1995–2014). Due to the scattered and uneven distribution of raw data points in both space and time (see Fig. 1a), a minimum of 2 samples per grid (25 × 25 km) was required for spatial averaging to achieve a climatological mean distribution of benthic biomass. Grids with mean biomass of 15.0 g C m^{-2} or higher (diamond markers) are deemed to be benthic biomass hotspots.

where the biological production producing them had occurred. On each day between Day 91 and 270 (April-September or roughly the productive seasons), a batch of particles ($n = 1923$) in the whole domain was released on the seafloor and backtracked to the sea surface to represent biogenic particles produced in spring and summer when ice algal and pelagic phytoplankton productions most likely occur. Particle locations were recorded and saved daily. The settling time and horizontal displacement (absolute geographical distance) were used to quantify the temporal and spatial scales for backtracked biogenic particles. Note that for the particle tracking simulations, we dealt only with the particles that initially settled to the bottom but ignored those resuspended and advected by strong currents later on.

2.5. Statistical analysis

A generalized additive model (GAM) was used to explore the potential associations between spatial patterns in benthic biomass and explanatory environmental variables derived from either the ice-ocean-biogeochemical model BIOMAS or the particle tracking model. The GAM is a nonparametric and additive regression technique to examine the relationships between dependent benthic biomass and a series of independent environmental predictors. The model used to describe the benthic biomass distribution was:

$$lnY_i = \beta + \sum_{j=1}^{p} s_j(X_{i,j}) + e_i$$

where lnY_i is a natural logarithm of benthic carbon biomass at the ith geographical location (g C m^{-2}), β is an intercept term, s is a thin plate spline regression function of an environmental predictor X, p is the total number of selected predictors, and e_i is an error term. A thin plate spline is a standard smoothing technique for GAM. The covariate points that are used to obtain the reduced basis are the 'knots' of the regression spline and the number of knots controls the model's flexibility (Wood, 2003). Here, a maximum of 5 knots is practically used.

All statistical analyses were conducted using the open-source statistical software package R (version 3.3.2) and the "mgcv" library for the GAM (Wood, 2006). We used the following model-derived environmental parameters that may be relevant to water mass characteristics, biological productivity, and benthic consumption: depth-integrated phytoplankton concentration, depth-integrated zooplankton concentration, ice algal concentration, bottom water temperature, bottom water salinity, sedimentation loss of PON, and horizontal displacement (i.e., total horizontal absolute distance while sinking in the vertical). To evaluate the significance of the above predictors, p-values and genuine cross-validation (GCV) scores were used to select predictors and models. A GAM was first fitted using all predictors and insignificant predictors ($p > 0.05$) were removed. The GAM was refitted iteratively until all remaining predictors were significant ($p < 0.05$) in the final optimized model.

3. Results

3.1. Benthic hotspot distributions

The benthic observations and hotspot distributions are only briefly described here. For detailed descriptions refer to Grebmeier et al. (2015a). Generally speaking, the five bounding boxes along the latitudinal gradient contained most of the confirmed hotspot regions denoted by the diamonds (>= 15.0 g C m^{-2}), although some exceptions exist (Fig. 5). For example, high biomass regions distributed to the north and southeast of the Chirikov box, and also between NECS and BC boxes. Moreover, the SCS, Chirikov, and BC boxes seem to have even higher biomasses than SLIP and NECS boxes. On average, the SCS, Chirikov, and BC hotspot boxes have nearly 50% more benthic biomass than the other two boxes (Grebmeier et al., 2015a).

3.2. Model validations

BIOMAS-simulated April-September climatological mean (1998–2014) ocean surface (0–15 m or upper 3 model layers) phytoplankton concentrations compared well with satellite-derived chlorophyll-a climatology for the same period (Fig. 6), with a high correlation coefficient ($r = 0.64$, $p < 0.001$), a near-zero mean bias (0.005 mg m^{-3}), and a small standard error (=0.01 mg m^{-3}). The model captured the main spatial patterns as shown by satellite imagery, with both revealing relatively high surface chlorophyll-a regions (>2.0 mg m^{-3}) extending from the Bering Sea shelf break through the Gulf of Anadyr, Anadyr Strait, Chirikov Basin, and Bering Strait to the southern Chukchi Sea. This band of elevated phytoplankton biomass concentration results from the influx of nutrient-rich Anadyr Water that supplies abundant nutrients for sustained biological productivity (Walsh et al., 1989; Springer et al., 1996). Overall, modeled surface chlorophyll-a concentrations were slightly higher than satellite-derived climatology and were exceptionally high (>4.0 mg m^{-3}) to the west of the Chirikov hotspot bounding box and south of the SCS hotspot bounding box (Fig. 6b).

Modeled annual total volume fluxes through the Bering Strait, as well as heat and freshwater fluxes, were compared with mooring-based estimations (Fig. 7). Modeled annual mean volume fluxes were correlated with mooring observations ($r = 0.65$, $p < 0.001$), with a mean bias of −0.23 Sv (model vs. observation: 0.67 vs. 0.90 Sv) and a standard error of 0.03 Sv (Fig. 7a). Modeled and observed heat fluxes also were correlated ($r = 0.82$, $p < 0.001$) with a mean bias of 1.5×10^{19} J and a standard error of 1.1×10^{19} J (Fig. 7b). Despite a high correlation between modeled and observed freshwater fluxes ($r = 0.87$, $p < 0.001$), modeled annual mean freshwater flux was only half of the observations (model vs. observation: 0.98 vs. 1.98×10^3 km^3; Fig. 7c). Additionally, model results revealed strong seasonality in volume, heat, and freshwater fluxes since peak northward transport occurred in the summertime whereas wintertime transport was low and occasionally reversed its direction to southward (see black curves in Fig. 7).

3.3. Modeled standing stocks of biological variables

BIOMAS-simulated 20-year climatological mean standing stocks of ice algae, phytoplankton, PON, and zooplankton demonstrate great spatial heterogeneity that is influenced by ice and light regimes, as well as hydrography (Fig. 8). Ice algae were high in coastal areas that frequently form polynyas, such as the Gulf of Anadyr and southwest of St. Lawrence Island, south of the Seward Peninsula, and along the northern coast of Alaska. In general, phytoplankton, PON, and zooplankton all have a south-north gradient and west-east asymmetry.

Model results also show distinctive features among the five hotspot

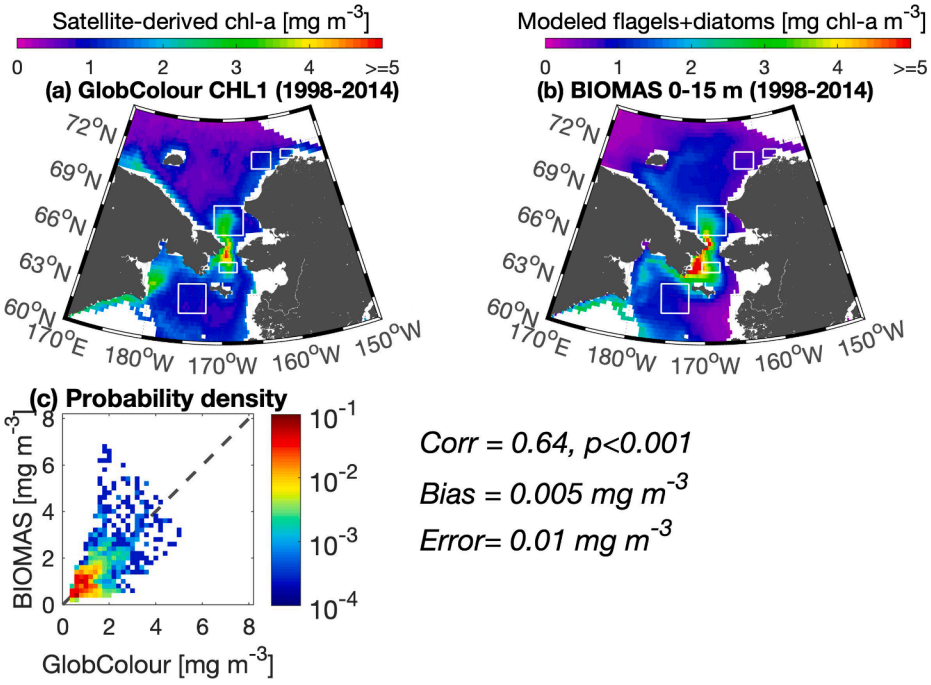

Fig. 6. Validation of modeled ocean surface phytoplankton concentration against satellite-retrieved chlorophyll-a concentration. (a) 17-year (1998–2014) April to September climatological mean GlobColour-derived chlorophyll-a concentration for Case-1 water (CHL1). (b) 17-year (1998–2014) climatological mean April to September BIOMAS-simulated 0–15 m (upper 3 vertical layers) phytoplankton (flagellates + diatoms) concentration, spatially interpolated to satellite data grid mesh. (c) Corresponding probability density distribution and statistical metrics between GlobColour-retrieved and BIOMAS-simulated chlorophyll-a concentrations. April-September months are chosen for calculating chlorophyll-a climatology because ocean color data are rarely available in October-March due to low light availability and/or ice cover. In panels (a) and (b), the coastal regions shallower than 20.0 m are masked as satellite chlorophyll-a signals may be contaminated by colored dissolved organic matter (CDOM) and/or total suspended matter (TSM) in the coastal waters (Blondeau-Patissier et al., 2014). Also, we used 0–15 m mean chlorophyll by averaging the model's upper three ocean vertical layers, rather than 0–5 m (only uppermost layer), because this depth range better represents ocean surface chlorophyll patterns of Case-1 water, which satellite ocean color sensors detect. The penetration depth of light is a function of wavelength and also depends on water types. It was estimated that the maximum mean penetration depth for broad wavelength sensors Band 4 (500–600 nm) is < 20 m (Gordon and McCluney, 1975). The correlation coefficient, mean bias, and standard error between satellite-retrieved and modeled chlorophyll-a are calculated.

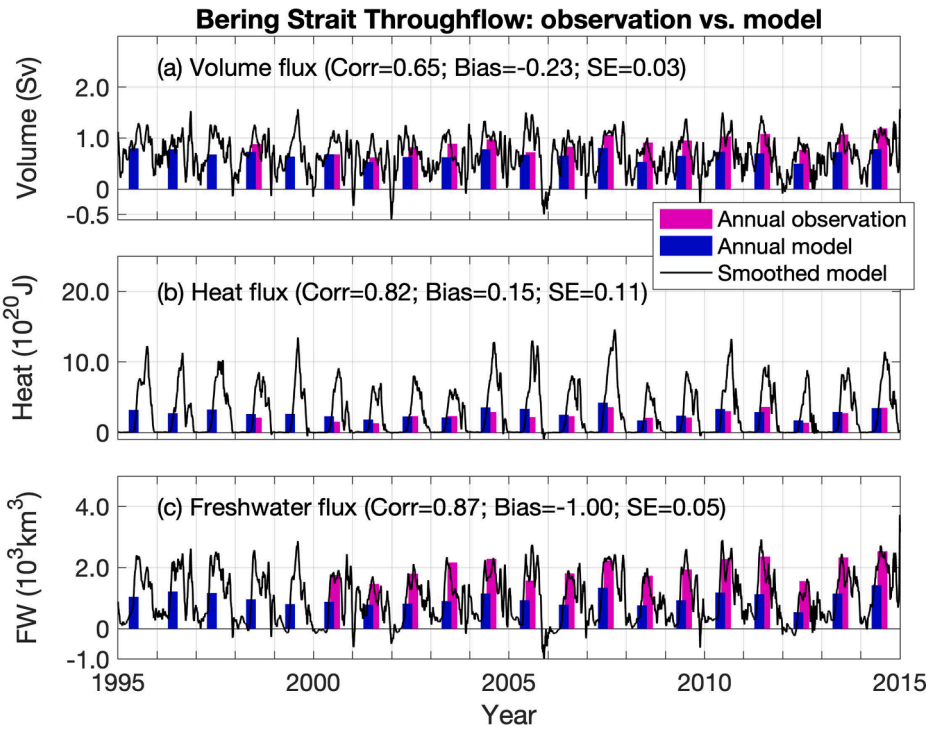

Fig. 7. Observation-model comparisons of Bering Strait throughflow: (a) total volume flux, (b) heat flux, and (c) freshwater flux. The vertical bars are calendar year mean quantities and black curves are 30-day moving averages of BIOMAS-derived daily fluxes.

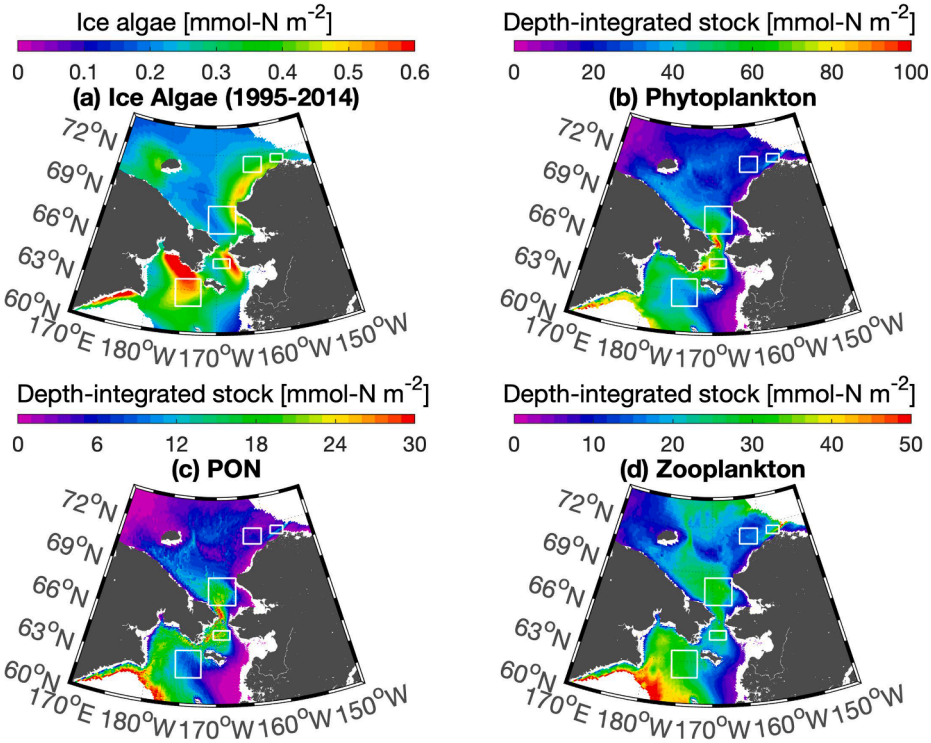

Fig. 8. BIOMAS-simulated 20-year climatological mean standing stocks on the northern Bering and Chukchi shelf in 1995–2014. (a) Ice algae, (b) depth-integrated phytoplankton, (c) depth-integrated particulate organic nitrogen, and (d) depth-integrated zooplankton. All variables are expressed in mmol-N m^{-2}.

subdomains. Modeled ice algal stocks are highest in SLIP, followed by NECS, Chirikov, and BC, and lowest in SCS (Fig. 8a). In comparison, phytoplankton and PON stocks are highest in SCS and Chirikov, moderate in SLIP and Barrow Canyon, and lowest in NECS (Fig. 8b and 8c). Zooplankton standing stock shows similar patterns as the phytoplankton in terms of west-east asymmetry although the south-north gradient seems smaller (Fig. 8d).

3.4. Biological versus physical contributions to particulate organic matter pool

The net biological versus physical (i.e., hydrographic) contributions to water column POM revealed likely distinctive food supply mechanisms for various benthic hotspots. Gross primary production (GPP) demonstrates strong west-east asymmetry primarily due to water mass characteristics and nutrient availability, as well as a south-north gradient due to ice-modulated light limitation (Fig. 9a), similar to the phytoplankton standing stock (Fig. 8b). Modeled GPP is the highest in the energetic Anadyr Strait and Bering Strait (~6.0 mol-N $m^{-2}yr^{-1}$ or equivalently ~ 480 gC $m^{-2}yr^{-1}$ using a Redfield C:N ratio of 106:16). Among all five hotspot subdomains, Chirikov has the highest annual GPP, followed by SCS and SLIP, while NECS and BC are much lower. PON sedimentation loss rates are much higher in the Chirikov and SCS hotspots compared to the other three hotspots (Fig. 9b). In the Anadyr Strait just upstream of the Chirikov subdomain, net biological rates of change for the POM stock are highest (positive) whereas physical-transport-induced net residual rates of change are lowest (negative) (Fig. 9c and 9d). Similarly, Bering Strait has high (positive) net biological rates and low (negative) net residual rates of change, indicative of net POM sources that supply to the downstream SCS hotspot. The BC region shows negative biological rates and positive residual rates of change for the POM stock, indicating POM funneling (convergence) from nearby shelf regions into the deep canyon. In comparison, net biological and residual rates of change are mostly neutral (approximately zero) in the SLIP and NECS hotpots, suggesting that those two hotspots are quasi-balanced in annual POM production and consumption in the water column, and that horizontal advection of POM has a minor impact in supplying SLIP and NECS hotspots.

3.5. Advective spatiotemporal scales of biogenic particles

Sinking velocity was a predominant factor in determining advective spatiotemporal scales for backward tracked particles that originated from known hotspot regions (Fig. 10). Particles of a 1 m d^{-1} sinking velocity have settling times and horizontal displacements 1–2 orders of magnitude longer than those with a sinking velocity of 100 m d^{-1} ones. Slow sinking particles (1 m d^{-1}) remained in the water for 1 to 3 months and were displaced by hundreds of km. In comparison, fast-sinking particles (100 m d^{-1}) quickly settled to the seafloor (≤1 day), with an advective spatial scale of 0.1–1 km among all 5 hotspots.

Drastic differences were also found among hotspot subdomains. For the SLIP and NECS subdomains, the majority of settled biogenic particles originated from nearby sources whereas particles settled to the three other hotspot domains traveled significantly longer distances, especially forw the slowest sinking particles of 1 m d^{-1} (Fig. 11). At 1 m d^{-1} (Fig. 11 upper panels), SLIP particles have the shortest displacement, followed by NECS particles, with both in the range of 100–150 km. Particles of the other three subdomains all have >200 km displacements, with SCS being the greatest (385.0 ± 126.9 km) among the five subdomains (Fig. 10b). Particles of fast sinking speed (e.g., 50 m d^{-1}) that settled in each bounding box all originated from local sources within the boxes regardless of hotspot subdomains (Fig. 11 lower panels).

3.6. Statistical analysis of benthic macrofaunal biomass distribution

The four significant predictors in an optimized GAM for fitting log-transformed benthic biomass are log-transformed depth-integrated phytoplankton concentration, log-transformed depth-integrated zooplankton concentration, PON sedimentation loss rate, and horizontal displacement for 10 m d^{-1} sinking particles, which together explain 47% of the total variance (adjusted $r^2 = 0.47$; $n = 133$). Generally, benthic biomass has a positive association with log-transformed phytoplankton concentration (Fig. 12a), implying that maintaining high benthic biomass requires moderately high water-column phytoplankton. The relationships between zooplankton biomass concentration and benthic biomass are bimodal (Fig. 12b). Benthic biomass has a generally negative association with PON sedimentation loss, which decreases in 0–500 mmol-N $m^{-2}yr^{-1}$, slightly increases in 500–1000 mmol-N $m^{-2}yr^{-1}$, and

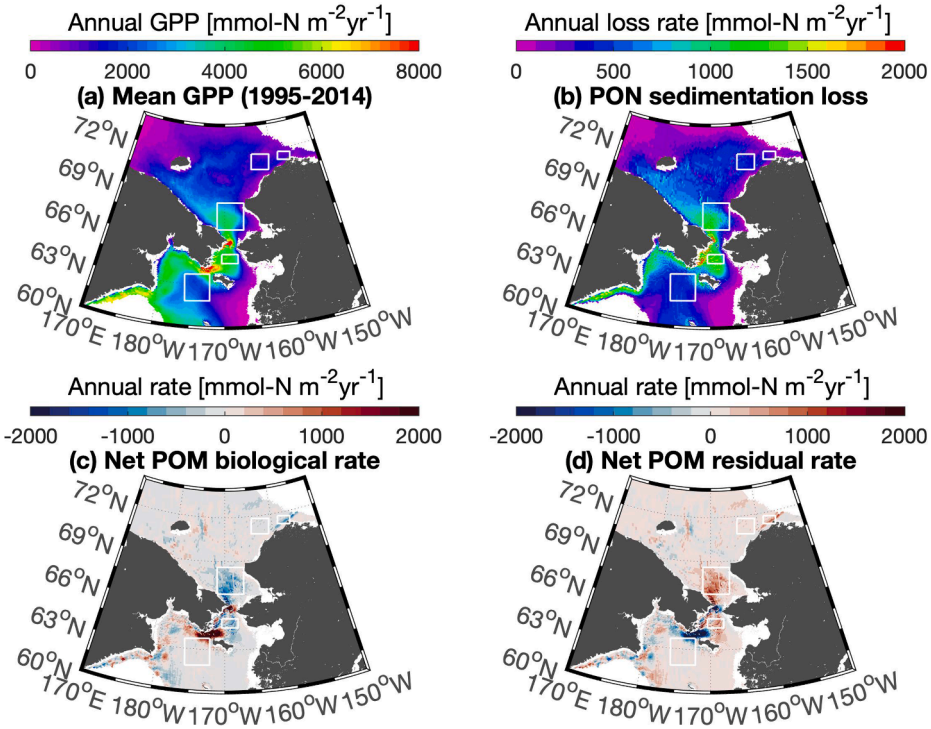

Fig. 9. BIOMAS-simulated annual rates on the northern Bering and Chukchi shelf in 1995–2014. (a) Gross primary productivity, (b) PON sedimentation loss, (c) net POM rate of change due to biological processes, and (d) net POM residual rate of change due to physical processes. All variables are annually and depth-integrated and expressed in mmol-N m^{-2} yr^{-1}.

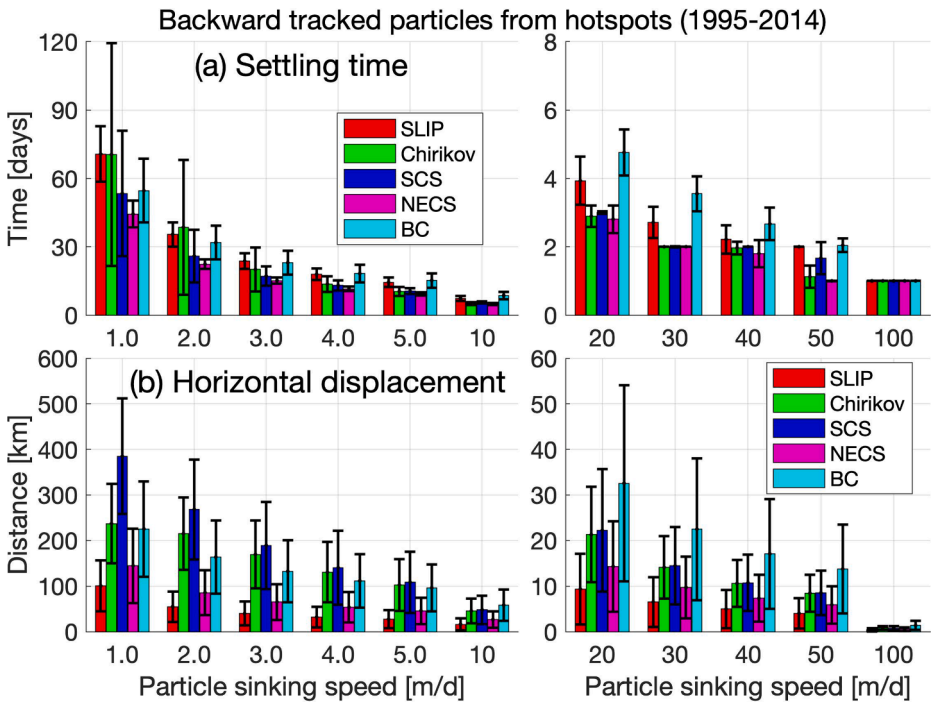

Fig. 10. Statistics for backtracked biogenic particles from 5 hotspot subdomains. (a) Settling time, and (b) horizontal displacement. Vertical bars and lines represent mean quantities and standard deviations. Note that y-axes on the left- and right-hand sides differ by one order of magnitude. Also, because particle time and locations are saved daily, the minimum time interval is 1 day.

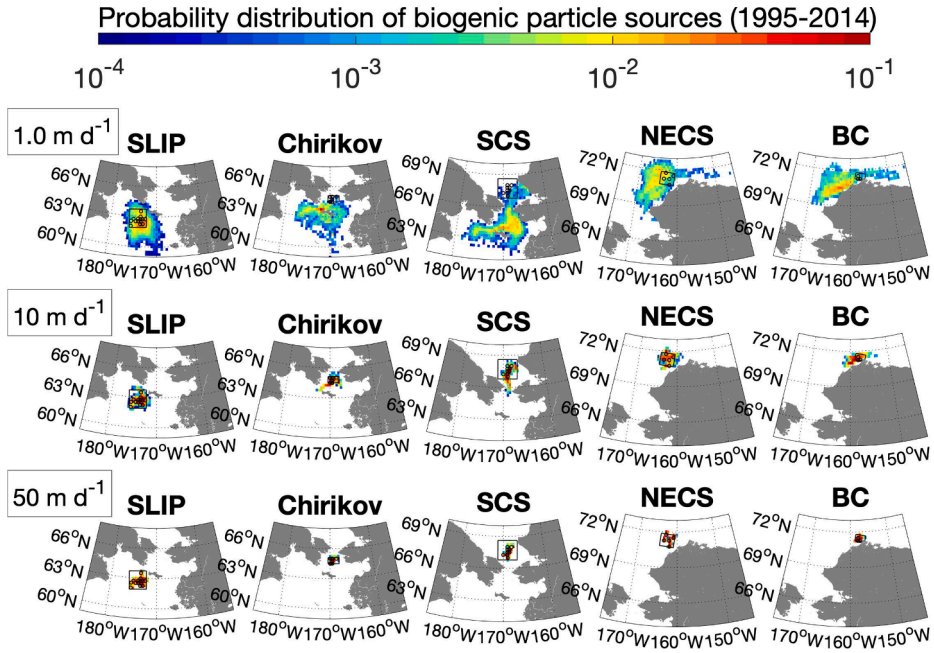

Fig. 11. Probability distribution of backtracked biogenic particles from confirmed hotspot regions of each subdomain. Cases for three representative sinking speeds are illustrated. Circles represent confirmed hotpot grids for illustrating probability distributions.

decreases again beyond 1000 mmol-N $m^{-2}yr^{-1}$ (Fig. 12c). Benthic biomass increases with displacement distance (Fig. 13d), suggesting that certain strong-flow regions are conducive for hotspot formation.

The GAM prediction based on those four environmental predictors fills in huge data gaps of benthic macroinfaunal biomass observation, notably in the data-limited Russian waters (compare Fig. 12e with Figs. 1a and 5). It captures known benthic hotspots on the northern Bering and Chukchi shelf (Fig. 12e). In addition, modeling results suggest the likelihood of a massive hotspot in the Gulf of Anadyr and smaller hotspots in the Herald Canyon (see Fig. 1a for corresponding locations) in Russian waters and to the southeast of SLIP in the central Bering shelf. The putative hotspot in the Gulf of Anadyr is located along the advective pathway for the nutrient-rich Anadyr Water (Walsh et al., 1989; Springer et al., 1996). Moreover, the GAM has variable predictive skills among five known hotspot subdomains. The model well represents Chirikov, SCS, and BC benthic biomasses, and its results are satisfactory

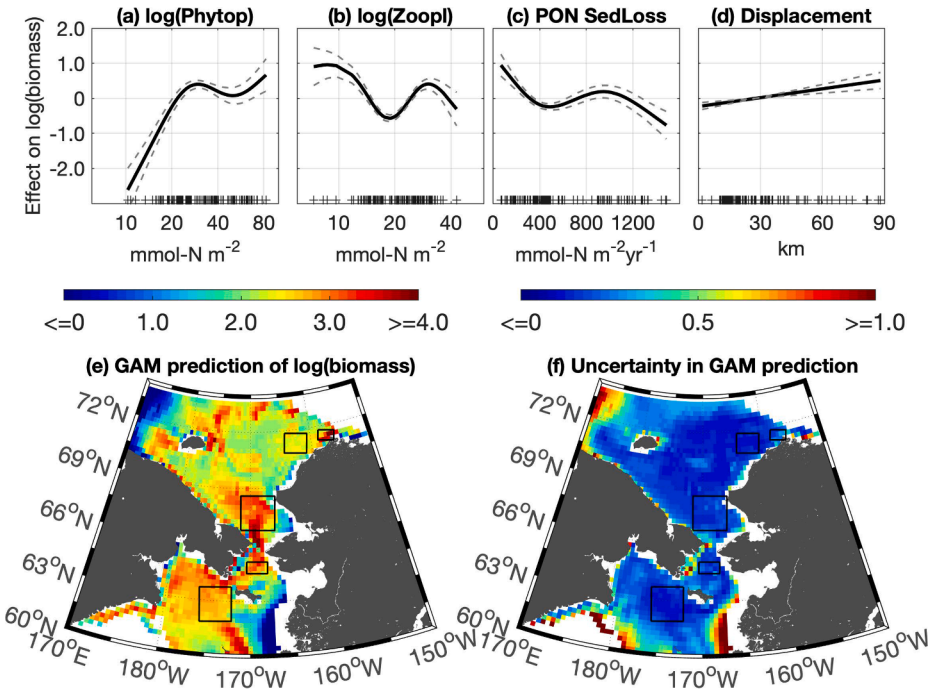

Fig. 12. Generalized additive model (GAM) results for benthic macroinfaunal biomass (g C m^{-2}) based on 4 environmental predictors. Additive effects of each one of the predictors on log-transformed benthic biomass: (a) log-transformed depth-integrated phytoplankton biomass concentration, (b) log-transformed depth-integrated zooplankton biomass concentration, (c) PON sedimentation loss rate, and (d) particle horizontal displacement. (e) GAM-predicted spatial distributions of macroinfaunal biomass using the above four environmental predictors. (f) Uncertainties associated with the GAM prediction. In panels a-d, solid curves are smoothed functional responses, dashed curves show standard errors, and black crosses are environmental predictor values used for model fitting. For panels e-f, color bars are illustrated in natural-logarithmically transformed benthic biomass.

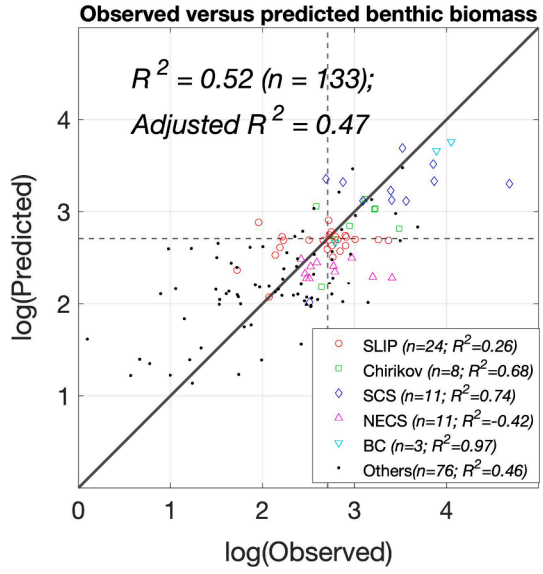

Fig. 13. Observed versus GAM-predicted benthic macroinfaunal biomasses inside the five hotspot bounding boxes and outside those boxes. The solid line denotes a perfect observation-model match, dashed lines indicate the hotspot threshold (15.0 g C m^{-2}), and colored markers represent various hotspot bounding boxes.

in the SLIP subdomain (Fig. 13). However, the GAM underestimates the benthic biomass in the NECS subdomain (see Fig. 13 magenta triangles).

4. Discussion

Decades of interdisciplinary studies have demonstrated that tight pelagic-benthic coupling and efficient carbon export (i.e., short food chains) in the high-latitude continental shelf ecosystem of the northern Bering and Chukchi seas support rich and diverse benthic communities and result in important feeding grounds for marine mammals and seabirds (e.g., Grebmeier and McRoy, 1989; Walsh et al., 1989; Dunton et al., 2005; Lalande et al., 2007; Grebmeier et al., 2015a, 2015b). Here, analyses of historic *in-situ* data and process-based and statistical modeling results explored the physical-biological processes driving the availability of food to benthic hotspots from the northern Bering Sea to the northeastern Chukchi Sea and further shed light on key environmental drivers for the hotspot formation. Based on these results, two contrasting regimes with differing biophysical mechanisms for the production of biogenic materials and subsequent transport to multiple benthic hotspots were identified in the Pacific Arctic region.

4.1. Local-supply regime

The SLIP and NECS subdomains can be categorized as local-supply regimes. Being situated in relatively weak ocean current fields as indicated by particle tracking results (Fig. 11b and 12), those two subdomains are predominantly fueled by locally produced carbon, which is supported by the neutral net biological and physical POM rates of change (Fig. 9c and 9d). Ice algal biomass, despite being 2–3 orders of magnitude lower than water column phytoplankton biomass (Fig. 8a and 8b), likely plays a more important role in supplying organic carbon to the benthos in those two subdomains than in the other three. The percentages of ice algae biomass to total standing stock, as well as ice algal GPP to total GPP, were much higher in SLIP and NECS than the other three subdomains (Fig. 14). However, even within the SLIP and NECS subdomains, modeled ice algal biomass and production only accounted for small proportions of the total biomass and production of the combined ice and water column primary producers. Because ice algae are formed early in the growing season and have fast sinking speeds after detachment from the ice substrate, zooplankton grazing loss is probably low and hence export efficiency is likely high (Gradinger, 2009; Leu et al., 2011; Boetius et al., 2013; Lalande et al., 2020). Furthermore, relatively low zooplankton biomass in the Bering and Chukchi seas in early spring may be insufficient to graze substantial proportions of the available primary production (Campbell et al., 2009, 2016). The relatively high ice algal production in SLIP and NECS subdomains is related to the winter-spring polynyas, within which ice growth can drive nutrient transport ("incorporate" nutrients) from surface water to the sea ice, maintain primary ice algal habitat near the nutrient-rich surface water, and therefore sustain ice algal productivity

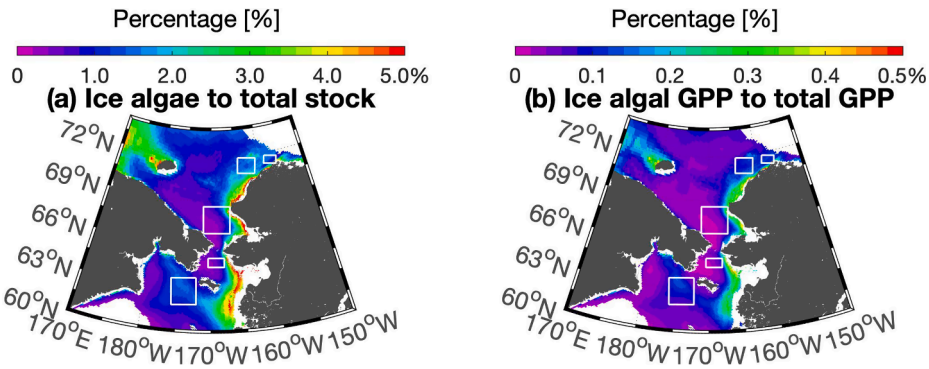

Fig. 14. BIOMAS-simulated sea ice algae contribution. (a) Ratio of ice algae to total primary producer (sum of ice algae and water column phytoplankton) standing stock. (b) Ratio of ice algal productivity to total gross primary productivity.

and biomass accumulation (Jin et al., 2006; Deal et al., 2011).

4.2. Advective regime

The Chirikov, SCS, and BC subdomains can be categorized as advective regimes. All three subdomains are influenced by topographically controlled flow fields (controlled by Anadyr Strait, Bering Strait, and Barrow Canyon, respectively), and biogenic particles representing phytoplankton cells and settling to those hotspots were advected long distances, on the order of hundreds of kilometers (Fig. 10b), and predominantly originated outside of their bounding boxes (Fig. 11 upper panels). Therefore, benthic hotspots of the advective regimes must rely heavily on biological production in upstream regions and the subsequent downstream deposition of that organic carbon, in addition to seasonal *in-situ* production. The most important feature among those subdomains is shown by the negative POM biological rate and positive residual rate of change (Fig. 9c and 9d), indicating that local biological consumption exceeds primary production. Hence, benthic hotspots in those subdomains must receive substantial transported POM from the upstream. Mooring and ship-based measurements in the SCS showed elevated chlorophyll-a concentrations (>1 mg m^{-3}) from May to September, likely sustained by both advected nutrients from the Bering Sea and locally regenerated nutrients through POM decomposition (Nishino et al., 2016).

In the BC subdomain, unlike the other two advective ones, elevated phytoplankton standing stock is caused primarily by flow convergence in the deep canyon (Pickart et al., 2019) so that upstream sources with high positive POM biological rates are not as prominent as in the Chirikov and SCS subdomains (Fig. 9c). For the BC and shelfbreak regions to the east of BC, video-plankton recorder measurements found exceptionally high concentrations of plankton and marine snow particles that were advected from the surrounding Chukchi shelf (Ashjian et al., 2005). Sediment trap data also revealed much higher particulate organic carbon (POC) export fluxes in Barrow Canyon than surrounding shelf regions (Lalande et al., 2007).

4.3. Putative hotspots inferred by modeling

Statistical GAM fitting and reconstruction of benthic macroinfaunal biomass generally reproduced the 4 known hotspots from the northern Bering to northeastern Chukchi shelf despite its underestimation of benthic biomass in the NECS (Fig. 12e). The GAM also inferred three putative hotspots in data-constrained regions: Gulf of Anadyr, Herald Canyon, and central Bering shelf (Fig. 12e). The putative hotspot in the Gulf of Anadyr is located north and northwest of the SLIP hotspot, under the large seasonal polynya in the region (Grebmeier and Cooper, 1995). A pilot cruise in the late 1980s sampled the region and found high macrofaunal benthic biomass, sediment oxygen consumption, and carbon accumulation in the western Gulf of Anadyr (Grebmeier, 1993). This putative hotspot is likely affected by nutrient-rich Anadyr Water and has relatively high phytoplankton standing stock (Fig. 8b), long particle displacement (Fig. 15a), and strong convergence/divergence of POM (Fig. 9c and 9d).

The statistical model predicted a second albeit less pronounced hotspot in the Herald Canyon region, which was confirmed by recent sampling efforts through the Russian-American Long-term Census of the Arctic (RUSALCA) Program (Denisenko et al., 2015; Grebmeier et al., 2015b; Pisareva et al., 2015). This putative hotspot may be formed similarly as the Barrow Canyon, both having moderately high phytoplankton and zooplankton stocks (Fig. 9b and 9d), low PON sedimentation loss (Fig. 10b), and relatively long particle displacement (Fig. 15a). A third putative hotspot in the central Bering shelf and southeast of the SLIP subdomain was also inferred by the GAM, although limited benthic data exist to either confirm or refute its presence.

4.4. Hotspot persistence and vulnerability in a rapidly changing Pacific Arctic region

The main purpose of our study was to evaluate biophysical drivers for food supplies to five benthic hotspot regions by using 20-year climatological results and without looking into the interannual variability and decadal trends of those drivers. Nevertheless, many other studies have documented marine ecosystem shifts and reorganization associated with the emergence of a "new normal" Arctic (e.g., Grebmeier et al., 2006b, 2018; Ardyna et al., 2014; Renaud et al., 2015; Feng et al., 2018). It has been speculated that certain regions might shift from a benthic-dominated to a pelagic-dominated ecosystem with a reduced export efficiency of under-ice and open-water biological production to the seafloor as Arctic sea ice continues to diminish (Piepenburg, 2005; Grebmeier, 2012; Wassman and Reigstad, 2011; Kędra et al., 2015; Moore et al., 2018). The interannual variability and decadal trends of physical transport rates (advection and sinking) and multiple biological rates (primary production, respiration, mortality, excretion, and zooplankton grazing) that all contribute to carbon export production will be analyzed in a follow-up study, along with the observed trends (Grebmeier et al., 2018).

Because of distinctive food supply mechanisms among 5 hotspot subdomains, local-supply regimes are likely more prone to ongoing environmental changes (notably sea ice loss and ocean warming) than advective regimes due to their reliance on locally generated production and high export efficiency. For the local-supply regimes, significant changes have already been detected in the SLIP subdomain. Time-series observations over 2 decades indicated that high benthic biomass centers of the SLIP hotspot have shifted northward and that common bivalve species have declined and replaced by polychaetes (Goethel et al., 2018; Grebmeier et al., 2018). Also, by synthesizing five time-series stations from 1998 to 2015, Grebmeier et al. (2018) concluded that although three southern stations have seen significant reductions in benthic

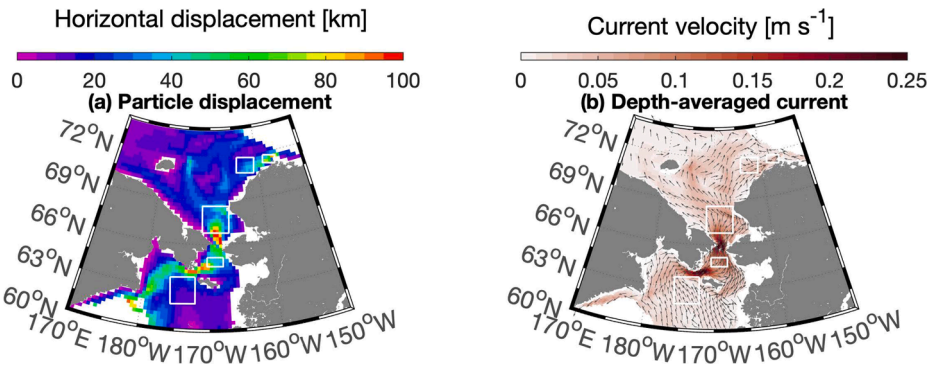

Fig. 15. (a) Mean horizontal displacement of biogenic particles with a constant sinking speed of 10.0 m d^{-1}. (b) BIOMAS-simulated depth-averaged ocean current. The colors indicate current velocities and superimposed vectors indicate current directions.

biomass since 2005, two northern ones had no significant trends and remained dominated by bivalves. One plausible explanation for the northward shift of the high biomass center was attributed to phytoplankton size structure changes during the post-bloom period that was inferred from satellite ocean color imagery (Waga et al., 2018).

Three subdomains categorized as advective regimes may have variable responses to environmental changes depending on the complex interactions between upstream biological production and physical transport processes. For instance, in the Chirikov subdomain, with three other time-series stations having no significant trends in benthic biomass, one station showed a significant declining trend in biomass as the dominant amphipods in 1999–2004 were replaced by bivalves after 2005 (Grebmeier et al., 2018). In comparison, SECS time-series stations showed overall upward trends in benthic biomass in 1998–2015, mainly driven by increasing bivalve populations over the last 5 years (Goethel et al., 2018; Grebmeier et al., 2018).

4.5. Model caveats and knowledge gaps

Although modeled climatological mean ocean currents represented overall circulation patterns in the Bering and Chukchi regions (Pickart et al., 2016, 2019), the ice-ocean-biogeochemical model could not well resolve the convergent flow patterns around the NECS hotspot (Fig. 15b), especially the multiple flow pathways for nutrient-rich winter water (Pickart et al., 2016) that have been suggested to sustain summertime primary productivity, which is a possible important driver for the formation of this hotspot (Feder et al., 1994; Lowry et al., 2015; Lin et al., 2019). This inability may have resulted from unresolved subgrid ocean dynamics and/or insufficient grid resolutions relative to the complex bottom topography of the region. Consequently, the GAM underestimated benthic biomasses at all available grid points within the NECS subdomain except one point (see Fig. 13 magenta triangles). Hence, the model results for this subdomain should be interpreted with caution. Notably recent field data indicated that the core of the NECS benthic hotspot is located further north and southeast of Hanna Shoal than our study results (Young et al., 2017).

Regarding GAM statistical modeling, the bimodal relationship between benthic biomass and zooplankton biomass seems difficult to explain. Benthic biomass is high in the low zooplankton biomass range and decreases with increasing zooplankton until 18 mmol-N m^{-2}, implying that low zooplankton biomass in the NECS subdomain (Fig. 8d) allows a significant proportion of organic matter reaching to the benthos without being heavily grazed by zooplankton. However, benthic biomass increases with zooplankton biomass in the 18–30 mmol-N m^{-2} range, mainly because all four other hotspot subdomains have moderately high zooplankton biomass of around 30 mmol-N m^{-2} (Fig. 8d). Therefore, the direct and indirect roles of zooplankton in benthic biomass distribution may need further investigations.

In addition, particle tracking simulations conducted in this study deal only with the initial settlement of biogenic particles that are produced in the water column and then delivered via vertical sinking and current-induced advection. However, other mechanisms, particularly bottom resuspension and subsequent lateral advection of settled particles, may play a role in the ultimate deposition of organic matter used by benthic organisms. A recent study examined spatial patterns of settled microalgae and sediment organic carbon (and associated benthic communities) relative to near-bottom current flows (derived from a high-resolution hydrodynamic model) in the SLIP and Chirikov hotspots (Lovvorn et al., 2020). That study concluded that patterns of sediment long-term organic carbon largely depended on near-bottom currents in the Chirikov region whereas regional depth gradient and bathymetry were the best predictors of the spatial patterns of sediment organic carbon in the SLIP region (Lovvorn et al., 2020).

The imbalance between POM export and benthic consumption may infer the presence and persistence of a sediment "food bank" that may buffer seasonal to interannual variations in pulsed ice and water column production and carbon export (Moran et al., 2005; Lepore et al., 2007). However, given that the present ice-pelagic ecosystem model is not coupled to a benthic ecology module, quantifying organic matter inventories at the seafloor that have been found to vary substantially in both time and space was not possible (Cooper et al., 2002, 2012; Grebmeier et al., 2015a). Instead, climatological mean standing stocks and rates of key biological variables were used to represent the total water column budget of organic matter (Fig. 8) and relevant rate contributions (Fig. 9). This allowed demonstration of differential food supply mechanisms for multiple hotspot subdomains. A future direction of research is to explicitly model benthic processes and to two-way couple a benthic biogeochemical model to the pelagic model. This will enable better quantification of a seasonally varying organic matter pool for the benthos and to further address how the sediment food bank may respond to contemporary and future environmental changes. A network model based on steady-state food web interactions across trophic levels suggested that required inputs of settling microalgae (food) exceeded satellite-derived primary production by as much as 50% in the SLIP and Chirikov hotspot regions (Lovvorn et al., 2015). The aforementioned modeling and synthesis of energetic data will provide heuristic guidance for formulating and parametrizing pelagic-benthic coupling relationships in future biogeochemical modeling efforts.

Also, by assuming a single constant PON sinking velocity (20 m d^{-1}) for the detritus component, the intermediate-complexity biogeochemical model for ice and pelagic ecosystems neglected processes pertinent to the formation of marine snow aggregates, and did not distinguish ice algal versus water column phytoplankton species. Ice algae may come off the ice as already formed marine snow aggregates and serve as a critical food source for benthos especially during springtime prior to the occurrence of pelagic phytoplankton blooms (Gradinger, 2009; Dunton et al., 2014; Selz et al., 2018). Particle tracking results suggested that fast-sinking marine snow particles of 50 and 100 m d^{-1} settled very

quickly after their formation and traveled very short distances regardless of locations (Figs. 10 and 11 lower panels).

Moreover, the overall quantity (inventory) of organic matter supply and the budget in the northern Bering and Chukchi seas were evaluated, but other environmental factors that may influence the distribution of the benthic communities were ignored, such as the quality of different food sources (fresh microalgae vs. detritus), and bottom resuspension. North et al. (2014) analyzed gut contents of five macrofaunal species (including 3 bivalves, 1 brittle star, and 1 polychaete) in the SLIP region. Their short-term data from gut contents suggested that bivalves and brittle stars responded to fresh algae more quickly than polychaetes, but stable isotope data indicated that fresh algae contributed little to overall carbon assimilated by those species in longer time scales. Also, resuspension of particles may contribute to elevated particulate organic carbon export across all Arctic shelves (Lalande et al., 2009; 2020). However, modeling resuspension processes requires resolving bottom boundary layer dynamics, which is beyond the scope of our study.

Finally, establishing long-term ecological research and maintaining annual sampling programs in this region is of critical importance in detecting where and when marine ecosystems are in transition and whether a "tipping point" has been reached so that certain ecosystems have been fundamentally altered from one state to another (Duarte et al., 2012; Grebmeier et al., 2018). The ongoing DBO and ASGARD (an acronym for Arctic Shelf Growth, Advection, Respiration, and Deposition) programs are two great examples of community efforts to monitor Pacific Arctic ecosystem change from physical and chemical environments, planktonic and benthic communities, to upper trophic level seabirds and mammals. Combining continuous time-series observations with conceptual and process-based models are imperative to achieve a system-level understanding of this sympagic-pelagic-benthic ecosystem and to develop a predictive capability of the rapidly changing Pacific Arctic region.

Declaration of Competing Interest

The authors declare that they have no known competing financial interests or personal relationships that could have appeared to influence the work reported in this paper.

Acknowledgements

This work was supported by the National Science Foundation Office of Polar Programs (1604047 to RJ, ZF, and CA, 1602985 and 1416920 to JZ, 1603466 to RC, 1603566 and 1702456 to JG) and the NASA Cryosphere Program (NNX15AG68G to CA, RC, and JZ). Dr. Paul Renaud and two anonymous reviewers provided insightful and constructive comments that significantly improved the quality and readability of the paper. We thank Kristina Kvile for helping with the statistical analysis, Rebecca Woodgate for sharing the Bering Strait throughflow data, and Ya Ping Wang for discussing bottom resuspension. WHOI's high-performance computing facility provided data storage and computational resources. Kate Lowry provided feedback for an earlier version of the manuscript and Natalie Renier assisted with the graphic abstract.

References

Amante, C., Eakins, B.W., 2009. ETOPO1 1 arc-minute Global Relief Model: procedures, data sources and analysis. NOAA technical memorandum NESDIS NGDC-24. National Geophysical Data Center, NOAA. doi:10.7289/V5C8276M.

Ardyna, M., Babin, M., Gosselin, M., Devred, E., Rainville, L., Tremblay, J.-E., 2014. Recent Arctic Ocean sea ice loss triggers novel fall phytoplankton blooms. Geophys. Res. Lett. 41, 6207–6212. https://doi.org/10.1002/2014GL061047.

Ashjian, C.J., Gallager, S.M., Plourde, S., 2005. Transport of plankton and particles between the Chukchi and Beaufort Seas during summer 2002, described using a Video Plankton Recorder. Deep-Sea Research Part II: Topical Studies in Oceanography 52, 3259–3280. https://doi.org/10.1016/j.dsr2.2005.10.012.

Blondeau-Patissier, D., Gower, J.F.R., Dekker, A.G., Phinn, S.R., Brando, V.E., 2014. A review of ocean color remote sensing methods and statistical techniques for the detection, mapping and analysis of phytoplankton blooms in coastal and open oceans. Prog. Oceanogr. 123, 23–144. https://doi.org/10.1016/j.pocean.2013.12.008.

Boetius, A., Albrecht, S., Bakker, K., Bienhold, C., Felden, J., Fernández-Méndez, M., Hendricks, S., Katlein, C., Lalande, C., Krumpen, T., Nicolaus, M., Peeken, I., Rabe, B., Rogacheva, A., Rybakova, E., Somavilla, R., Wenzhöfer, F., 2013. Export of algal biomass from the melting Arctic sea ice. Science 339, 1430–1432. https://doi.org/10.1126/science.1231346.

Campbell, R.G., Sherr, E.B., Ashjian, C.J., Plourde, S., Sherr, B.F., Hill, V., Stockwell, D. A., 2009. Mesozooplankton prey preference and grazing impact in the western Arctic Ocean. Deep Sea Res. Part II 56, 1274–1289. https://doi.org/10.1016/j.dsr2.2008.10.027.

Campbell, R.G., Ashjian, C.J., Sherr, E.B., Sherr, B.F., Lomas, M.W., Ross, C., Alatalo, P., Gelfman, C., Keuren, D.V., 2016. Mesozooplankton grazing during spring sea-ice conditions in the eastern Bering Sea. Deep-Sea Research Part II: Topical Studies in Oceanography 134, 157–172. https://doi.org/10.1016/j.dsr2.2015.11.003.

Coachman, L.K., Aagaard, K., 1988. Transports through Bering Strait: Annual and interannual variability. J. Geophys. Res. Oceans 93, 15535–15539. https://doi.org/10.1029/JC093iC12p15535.

Cooper, L.W., Grebmeier, J.M., Larsen, I.L., Egorov, V.G., Theodorakis, C., Kelly, H.P., Lovvorn, J.R., 2002. Seasonal variation in sedimentation of organic materials in the St. Lawrence Island polynya region. Bering Sea. Marine Ecology Progress Series 226, 13–26. https://doi.org/10.3354/meps226013.

Cooper, L.W., Janout, M.A., Frey, K.E., Pirtle-Levy, R., Guarinello, M.L., Grebmeier, J.M., Lovvorn, J.R., 2012. The relationship between sea ice break-up, water mass variation, chlorophyll biomass, and sedimentation in the northern Bering Sea. Deep-Sea Research Part II: Topical Studies in Oceanography 65–70, 141–162. https://doi.org/10.1016/j.dsr2.2012.02.002.

Duarte, C.M., Lenton, T.M., Wadhams, P., Wassmann, P., 2012. Abrupt climate change in the Arctic. Nat. Clim. Change 2, 60–62. https://doi.org/10.1038/nclimate1386.

Deal, C., Jin, M., Elliott, S., Hunke, E., Maltrud, M., Jeffery, N., 2011. Large-scale modeling of primary production and ice algal biomass within arctic sea ice in 1992. J. Geophys. Res. 116, C07004. https://doi.org/10.1029/2010JC006409.

Denisenko, S.G., Grebmeier, J.M., Cooper, L.W., 2015. Assessing Bioresources and Standing Stock of Zoobenthos (Key Species, High Taxa, Trophic Groups) in the Chukchi Sea. Oceanography 28, 146–157. https://doi.org/10.5670/oceanog.2015.63.

Devol, A.H., Codispotit, L.A., Christensen, J.P., 1997. Summer and winter denitrification rates in western Arctic shelf sediments. Cont. Shelf Res. 17, 1029–1050. https://doi.org/10.1016/S0278-4343(97)00003-4.

Dunton, K.H., Goodall, J.L., Schonberg, S.V., Grebmeier, J.M., Maidment, D.R., 2005. Multi-decadal synthesis of benthic-pelagic coupling in the western arctic: Role of cross-shelf advective processes. Deep-Sea Research Part II: Topical Studies in Oceanography 52, 3462–3477. https://doi.org/10.1016/j.dsr2.2005.09.007.

Dunton, K.H., Grebmeier, J.M., Trefry, J.H., 2014. The benthic ecosystem of the northeastern Chukchi Sea: An overview of its unique biogeochemical and biological characteristics. Deep-Sea Research Part II: Topical Studies in Oceanography 102, 1–8. https://doi.org/10.1016/j.dsr2.2014.01.001.

Feder, H.M., Naidu, A.S., Jewett, S.C., Hameedi, J.M., Johnson, W.R., Whitledge, T.E., 1994. The northeastern Chukchi Sea: Benthos-environmental interactions. Mar. Ecol. Prog. Ser. 111, 171–190. https://doi.org/10.3354/meps111171.

Feng, Z., Ji, R., Campbell, R.G., Ashjian, C.J., Zhang, J., 2016. Early ice retreat and ocean warming may induce copepod biogeographic boundary shifts in the Arctic Ocean. J. Geophys. Res. Oceans 121, 6137–6158. https://doi.org/10.1002/2016JC011784.

Feng, Z., Ji, R., Ashjian, C., Campbell, R., Zhang, J., 2018. Biogeographic responses of the copepod *Calanus glacialis* to a changing Arctic marine environment. Glob. Change Biol. 24, 159–170. https://doi.org/10.1111/gcb.13890.

Fennel, K., Wilkin, J., Levin, J., Moisan, J., O'Reilly, J., Haidvogel, D., 2006. Nitrogen cycling in the Middle Atlantic Bight: Results from a three-dimensional model and implications for the North Atlantic nitrogen budget. Global Biogeochem. Cycles 20 (GB3007), 1–14. https://doi.org/10.1029/2005GB002456.

Goethel, C.L., Grebmeier, J.M., Cooper, L.W., 2018. Changes in abundance and biomass of the bivalve Macoma calcarea in the northern Bering Sea and the southeastern Chukchi Sea from 1998 to 2014, tracked through dynamic factor analysis models. Deep-Sea Research Part II: Topical Studies in Oceanography 1–10. https://doi.org/10.1016/j.dsr2.2018.10.007.

Gordon, H.R., McCluney, W.R., 1975. Estimation of depth of sunlight penetration in sea for remote sensing. Appl. Opt. 14 (2), 413–416.

Gradinger, R., 2009. Sea-ice algae: Major contributors to primary production and algal biomass in the Chukchi and Beaufort Seas during May/June 2002. Deep Sea Res. Part II 56, 1201–1212. https://doi.org/10.1016/j.dsr2.2008.10.016.

Grebmeier, J.M., 1993. Studies of pelagic-benthic coupling extended onto the Soviet continental shelf in the northern Bering and Chukchi seas. Cont. Shelf Res. 13, 653–668. https://doi.org/10.1016/0278-4343(93)90098-I.

Grebmeier, J.M., 2012. Shifting patterns of life in the Pacific Arctic and Sub-Arctic Seas. Ann. Rev. Mar. Sci. 4, 63–78. https://doi.org/10.1146/annurev-marine-120710-100926.

Grebmeier, J.M., McRoy, C.P., 1989. Pelagic-benthic coupling on the shelf of the northern Bering and Chukchi Seas. III. Food Supply and Carbon Cycling. Mar. Ecol. Prog. Ser. 53, 79–91.

Grebmeier, J.M., Cooper, L.W., 1995. Influence of the St. Lawrence Island Polynya upon the Bering Sea benthos. J. Geophys. Res. 100, 4439–4460. https://doi.org/10.1029/94JC02198.

Grebmeier, J.M., Cooper, L.W., 2014. PacMARS Benthic Infaunal Parameters. Version 1.0. NCAR/UCAR EOL data. https://doi.org/10.5065/D6H70CVR.

Grebmeier, J.M., Cooper, L.W., 2018a. Benthic macroinfaunal samples collected from the Canadian Coast Guard Ship (CCGS) Sir Wilfrid Laurier, Northern Bering Sea to Chukchi Sea, 2013. Arctic Data Center. https://doi.org/10.18739/A2V11VK2K.

Grebmeier, J.M., Cooper, L.W., 2018b. Benthic Macroinfaunal Samples Collected from the Canadian Coast Guard Ship (CCGS) Sir Wilfrid Laurier 2014, Northern Bering Sea to Chukchi Sea. Arctic Data Center. https://doi.org/10.18739/A2KK94B8Q.

Grebmeier, J.M., Cooper, L.W., Feder, H.M., Sirenko, B.I., 2006a. Ecosystem dynamics of the Pacific-influenced Northern Bering and Chukchi Seas in the Amerasian Arctic. Prog. Oceanogr. 71, 331–361. https://doi.org/10.1016/j.pocean.2006.10.001.

Grebmeier, J.M., Overland, J.E., Moore, S.E., Farley, E.V., Carmack, E.C., Cooper, L.W., Frey, K.E., Helle, J.H., McLaughlin, F.A., McNutt, S.L., 2006b. A major ecosystem shift in the northern Bering Sea. Science 311, 1461–1464. https://doi.org/10.1126/science.1121365.

Grebmeier, J.M., Bluhm, B.A., Cooper, L.W., Danielson, S.L., Arrigo, K.R., Blanchard, A. L., Clarke, J.T., Day, R.H., Frey, K.E., Gradinger, R.R., Kędra, M., Konar, B., Kuletz, K. J., Lee, S.H., Lovvorn, J.R., Norcross, B.L., Okkonen, S.R., 2015a. Ecosystem characteristics and processes facilitating persistent macrobenthic biomass hotspots and associated benthivory in the Pacific Arctic. Prog. Oceanogr. 136, 92–114. https://doi.org/10.1016/j.pocean.2015.05.006.

Grebmeier, J.M., Bluhm, B.A., Cooper, L.W., Denisenko, S.G., Iken, K., Kedra, M., Serratos, C., 2015b. Time-series benthic community composition and biomass and associated environmental characteristics in the Chukchi Sea during the RUSALCA 2004–2012 program. Oceanography 28, 116–133. https://doi.org/10.5670/oceanog.2015.61.

Grebmeier, J.M., Frey, K.E., Cooper, L., Kędra, M., 2018. Trends in benthic macrofaunal populations, seasonal sea ice persistence, and bottom water temperatures in the Bering Strait region. Oceanography 31, 136–151. https://doi.org/10.5670/oceanog.2018.224.

Iken, K., Bluhm, B., Dunton, K., 2010. Benthic food-web structure under differing water mass properties in the southern Chukchi Sea. Deep-Sea Research Part II: Topical Studies in Oceanography 57, 71–85. https://doi.org/10.1016/j.dsr2.2009.08.007.

Jin, M., Deal, C.J., Wang, J., Shin, K.-H., Tanaka, N., Whitledge, T.E., Lee, S.H., Gradinger, R.R., 2006. Controls of the landfast ice–ocean ecosystem offshore Barrow, Alaska. Ann. Glaciol. 44, 63–72. https://doi.org/10.3189/172756406781811709.

Jin, M., Popova, E.E., Zhang, J., Ji, R., Pendleton, D., Varpe, Ø., Yool, A., Lee, Y.J., 2016. Ecosystem model intercomparison of under-ice and total primary production in the Arctic Ocean. J. Geophys. Res. Oceans 121, 934–948. https://doi.org/10.1002/2015JC011183.

Kędra, M., Moritz, C., Choy, E.S., David, C., Degen, R., Duerksen, S., Ellingsen, I., Górska, B., Grebmeier, J.M., Kirievskaya, D., van Oevelen, D., Piwosz, K., Samuelsen, A., Węsławski, J.M., 2015. Status and trends in the structure of Arctic benthic food webs. Polar Res. 34 https://doi.org/10.3402/polar.v34.23775.

Kishi, M.J., Kashiwai, M., Ware, D.M., Megrey, B. A., Eslinger, D.L., Werner, F.E., Noguchi-Aita, M., Azumaya, T., Fujii, M., Hashimoto, S., Huang, D., Iizumi, H., Ishida, Y., Kang, S., Kantakov, G. a., Kim, H., Komatsu, K., Navrotsky, V. V., Smith, S. L., Tadokoro, K., Tsuda, A., Yamamura, O., Yamanaka, Y., Yokouchi, K., Yoshie, N., Zhang, J., Zuenko, Y.I., Zvalinsky, V.I., 2007. NEMURO—a lower trophic level model for the North Pacific marine ecosystem. Ecological Modelling 202, 12–25. doi:10.1016/j.ecolmodel.2006.08.021.

Lalande, C., Grebmeier, J.M., Wassmann, P., Cooper, L.W., Flint, M.V., Sergeeva, V.M., 2007. Export fluxes of biogenic matter in the presence and absence of seasonal sea ice cover in the Chukchi Sea. Cont. Shelf Res. 27, 2051–2065. https://doi.org/10.1016/j.csr.2007.05.005.

Lalande, C., Forest, A., Barber, D.G., Gratton, Y., Fortier, L., 2009. Variability in the annual cycle of vertical particulate organic carbon export on Arctic shelves: Contrasting the Laptev Sea, Northern Baffin Bay and the Beaufort Sea. Cont. Shelf Res. 29, 2157–2165. https://doi.org/10.1016/j.csr.2009.08.009.

Lalande, C., Grebmeier, J.M., Hopcroft, R.R., Danielson, S.L., 2020. Annual cycle of export fluxes of biogenic matter near Hanna Shoal in the northeast Chukchi Sea. Deep-Sea Research Part II: Topical Studies in Oceanography. doi:10.1016/j.dsr2.2020.104730.

Lee, Y.J., Matrai, P.A., Friedrichs, M.A.M., Saba, V.S., Aumont, O., Babin, M., Buitenhuis, E.T., Chevallier, M., de Mora, L., Dessert, M., Dunne, J.P., Ellingsen, I.H., Feldman, D., Frouin, R., Gehlen, M., Gorgues, T., Ilyina, T., Jin, M., John, J.G., Lawrence, J., Manizza, M., Menkes, C.E., Perruche, C., Le Fouest, V., Popova, E.E., Romanou, A., Samuelsen, A., Schwinger, J., Séférian, R., Stock, C.A., Tjiputra, J., Tremblay, L.B., Ueyoshi, K., Vichi, M., Yool, A., Zhang, J., 2016. Net primary productivity estimates and environmental variables in the Arctic Ocean: An assessment of coupled physical-biogeochemical models. J. Geophys. Res. Oceans 121, 8635–8669. https://doi.org/10.1002/2016JC011993.

Lepore, K., Moran, S.B., Grebmeier, J.M., Cooper, L.W., Lalande, C., Maslowski, W., Hill, V., Bates, N.R., Hansell, D.A., Mathis, J.T., Kelly, R.P., 2007. Seasonal and interannual changes in particulate organic carbon export and deposition in the Chukchi Sea. J. Geophys. Res. 112, 1–14. https://doi.org/10.1029/2006JC003555.

Leu, E., Søreide, J.E., Hessen, D.O., Falk-Petersen, S., Berge, J., 2011. Consequences of changing sea-ice cover for primary and secondary producers in the European Arctic shelf seas: Timing, quantity, and quality. Prog. Oceanogr. 90, 18–32. https://doi.org/10.1016/j.pocean.2011.02.004.

Lin, P., Pickart, R.S., McRaven, L.T., Arrigo, K.R., Bahr, F., Lowry, K.E., Stockwell, D.A., Mordy, C.W., 2019. Water Mass Evolution and Circulation of the Northeastern Chukchi Sea in Summer: Implications for Nutrient Distributions. J. Geophys. Res. Oceans. https://doi.org/10.1029/2019JC015185.

Lindsay, R.W., Zhang, J., 2006. Assimilation of Ice Concentration in an Ice-Ocean Model. J. Atmos. Oceanic Technol. 23, 742–749.

Lovvorn, J.R., Jacob, U., North, C.A., Kolts, J.M., Grebmeier, J.M., Cooper, L.W., Cui, X., 2015. Modeling spatial patterns of limits to production of deposit-feeders and ectothermic predators in the northern Bering Sea. Estuar. Coast. Shelf Sci. 154, 19–29. https://doi.org/10.1016/j.ecss.2014.12.020.

Lovvorn, J.R., North, C.A., Kolts, J.M., Grebmeier, J.M., Cooper, L.W., Cui, X., 2016. Projecting the effects of climate-driven changes in organic matter supply on benthic food webs in the northern Bering Sea. Mar. Ecol. Prog. Ser. 548, 11–30. https://doi.org/10.3354/meps11651.

Lovvorn, J.R., Rocha, A.R., Danielson, S.L., Cooper, L.W., Grebmeier, J.M., Hedstrom, K. S., 2020. Predicting sediment organic carbon and related food web types from a physical oceanographic model on a subarctic shelf. Mar. Ecol. Prog. Ser. 633, 37–54. https://doi.org/10.3354/meps13163.

Lowry, K.E., Pickart, R.S., Mills, M.M., Brown, Z.W., van Dijken, G.L., Bates, N.R., Arrigo, K.R., 2015. The influence of winter water on phytoplankton blooms in the Chukchi Sea. Deep-Sea Research Part II: Topical Studies in Oceanography 118, 53–72. https://doi.org/10.1016/j.dsr2.2015.06.006.

Manda, A., Hirose, N., Yanagi, T., 2005. Feasible method for the assimilation of satellite-derived SST with an ocean circulation model. J. Atmos. Oceanic Technol. 22, 746–756. https://doi.org/10.1175/JTECH1744.1.

Maritorena, S., Siegel, D.A., 2005. Consistent merging of satellite ocean color data sets using a bio-optical model. Remote Sens. Environ. 94, 429–440. https://doi.org/10.1016/j.rse.2004.08.014.

Maritorena, S., D'Andon, O.H.F., Mangin, A., Siegel, D.A., 2010. Merged satellite ocean color data products using a bio-optical model: Characteristics, benefits and issues. Remote Sens. Environ. 114, 1791–1804. https://doi.org/10.1016/j.rse.2010.04.002.

Miklasz, K.A., Denny, M.W., 2010. Diatom sinking speeds: Improved predictions and insight from a modified Stokes' law. Limnol. Oceanogr. 55, 2513–2525. https://doi.org/10.4319/lo.2010.55.6.2513.

Moore, S.E., Grebmeier, J.M., 2018. The distributed biological observatory: linking physics to biology in the Pacific Arctic Region. Arctic 71, 1–7.

Moore, S.E., Stabeno, P.J., Grebmeier, J.M., Okkonen, S.R., 2018. The Arctic Marine Pulses Model: linking annual oceanographic processes to contiguous ecological domains in the Pacific Arctic. Deep Sea Res. Part II 152, 8–21. https://doi.org/10.1016/j.dsr2.2016.10.011.

Moran, S.B., Kelly, R.P., Hagstrom, K., Smith, J.N., Grebmeier, J.M., Cooper, L.W., Cota, G.F., Walsh, J.J., Bates, N.R., Hansell, D. a., Maslowski, W., Nelson, R.P., Mulsow, S., 2005. Seasonal changes in POC export flux in the Chukchi Sea and implications for water column-benthic coupling in Arctic shelves. Deep-Sea Research Part II: Topical Studies in Oceanography 52, 3427–3451. doi:10.1016/j.dsr2.2005.09.011.

Nishino, S., Kikuchi, T., Fujiwara, A., Hirawake, T., Aoyama, M., 2016. Water mass characteristics and their temporal changes in a biological hotspot in the southern Chukchi Sea. Biogeosciences 13, 2563–2578. https://doi.org/10.5194/bg-13-2563-2016.

North, C.A., Lovvorn, J.R., Kolts, J.M., Brooks, M.L., Cooper, L.W., Grebmeier, J.M., 2014. Deposit-feeder diets in the Bering Sea: Potential effects of climatic loss of sea ice-related microalgal blooms. Ecol. Appl. 24, 1525–1542. https://doi.org/10.1890/13-0486.1.

Nurser, A.J.G., Bacon, S., 2014. The Rossby radius in the arctic ocean. Ocean Sci. 10, 967–975. https://doi.org/10.5194/os-10-967-2014.

Pickart, R.S., Moore, G.W.K., Mao, C., Bahr, F., Nobre, C., Weingartner, T.J., 2016. Circulation of winter water on the Chukchi shelf in early Summer. Deep-Sea Research Part II: Topical Studies in Oceanography 130, 56–75. https://doi.org/10.1016/j.dsr2.2016.05.001.

Pickart, R.S., Nobre, C., Lin, P., Arrigo, K.R., Ashjian, C.J., Berchok, C., Cooper, L.W., Grebmeier, J.M., Hartwell, I., He, J., Itoh, M., Kikuchi, T., Nishino, S., Vagle, S., 2019. Seasonal to mesoscale variability of water masses and atmospheric conditions in Barrow Canyon, Chukchi Sea. Deep-Sea Research Part II: Topical Studies in Oceanography 162, 32–49.

Pirtle-Levy, R., Grebmeier, J.M., Cooper, L.W., Larsen, I.L., 2009. Chlorophyll a in Arctic sediments implies long persistence of algal pigments. Deep-Sea Research Part II: Topical Studies in Oceanography 56, 1326–1338. https://doi.org/10.1016/j.dsr2.2008.10.022.

Piepenburg, D., 2005. Recent research on Arctic benthos: Common notions need to be revised. Polar Biol. 28, 733–755. https://doi.org/10.1007/s00300-005-0013-5.

Pisareva, M.N., Pickart, R.S., Iken, K., Ershova, E.A., Grebmeier, J.M., Cooper, L.W., Bluhm, B.A., Nobre, C., Hopcroft, R.R., Hu, H.G., Wang, J., Ashjian, C.J., Kosobokova, K.N., Whitledge, T.E., 2015. The relationship between patterns of benthic fauna and zooplankton in the Chukchi Sea and physical forcing. Oceanography 28, 68–83. https://doi.org/10.5670/oceanog.2015.58.

Popova, E.E., Yool, A., Coward, A.C., Dupont, F., Deal, C., Elliott, S., Hunke, E., Jin, M., Steele, M., Zhang, J., 2012. What controls primary production in the Arctic Ocean? Results from an intercomparison of five general circulation models with biogeochemistry. J. Geophys. Res. 117, C00D12. https://doi.org/10.1029/2011JC007112.

Renaud, P.E., Sejr, M.K., Bluhm, B.A., Sirenko, B., Ellingsen, I.H., 2015. The future of Arctic benthos: Expansion, invasion, and biodiversity. Prog. Oceanogr. 139, 244–257. https://doi.org/10.1016/j.pocean.2015.07.007.

Saha, S., Moorthi, S., Pan, H.L., Wu, X., Wang, J., Nadiga, S., Tripp, P., Kistler, R., Woollen, J., Behringer, D., Liu, H., Stokes, D., Grumbine, R., Gayno, G., Wang, J., Hou, Y.T., Chuang, H.Y., Juang, H.M.H., Sela, J., Iredell, M., Treadon, R., Kleist, D., Van Delst, P., Keyser, D., Derber, J., Ek, M., Meng, J., Wei, H., Yang, R., Lord, S., Van Den Dool, H., Kumar, A., Wang, W., Long, C., Chelliah, M., Xue, Y., Huang, B., Schemm, J.K., Ebisuzaki, W., Lin, R., Xie, P., Chen, M., Zhou, S., Higgins, W., Zou, C. Z., Liu, Q., Chen, Y., Han, Y., Cucurull, L., Reynolds, R.W., Rutledge, G., Goldberg, M., 2010. The NCEP climate forecast system reanalysis. Bull. Am. Meteorol. Soc. 91, 1015–1057. https://doi.org/10.1175/2010BAMS3001.1.

Schweiger, A.J., Zhang, J., 2015. Accuracy of short-term sea ice drift forecasts using a coupled ice-ocean model. J. Geophys. Res. Oceans 120, 7827–7841. https://doi.org/10.1002/2015JC011273.

Selz, V., Laney, S., Arnsten, A.E., Lewis, K.M., Lowry, K.E., Joy-Warren, H.L., Mills, M.M., van Dijken, G.L., Arrigo, K.R., 2018. Ice algal communities in the Chukchi and Beaufort Seas in spring and early summer: Composition, distribution, and coupling with phytoplankton assemblages. Limnol. Oceanogr. 63, 1109–1133. https://doi.org/10.1002/lno.10757.

Springer, A.M., McRoy, C.P., Flint, M.V., 1996. The Bering Sea: shelf-edge processes and ecosystem production. Fish. Oceanogr. 5, 205–223. https://doi.org/10.1111/j.1365-2419.1996.tb00118.x.

Soetaert, K., Middelburg, J.J., Herman, P.M.J., Buis, K., 2000. On the coupling of benthic and pelagic biogeochemical models. Earth-Sci. Rev. 51, 173–201.

Waga, H., Hirawake, T., Fujiwara, A., Grebmeier, J.M., Saitoh, S.I., 2018. Impact of spatiotemporal variability in phytoplankton size structure on benthic macrofaunal distribution in the Pacific Arctic. Deep-Sea Research Part II: Topical Studies in Oceanography. doi:10.1016/j.dsr2.2018.10.008.

Walsh, J.J., McRoy, C.P., Coachman, L.K., Goering, J.J., Nihoul, J.J., Whitledge, T.E., Blackburn, T.H., Parker, P.L., Wirick, C.D., Shuert, P.G., Grebmeier, J.M., Springer, A.M., Tripp, R.D., Hansell, D.A., Djenidi, S., Deleersnijder, E., Henriksen, K., Lund, B.A., Andersen, P., Müller-Karger, F.E., Dean, K., 1989. Carbon and nitrogen cycling within the Bering/Chukchi Seas: Source regions for organic matter effecting AOU demands of the Arctic Ocean. Prog. Oceanogr. 22, 277–359. https://doi.org/10.1016/0079-6611(89)90006-2.

Wassmann, P., Reigstad, M., 2011. Future Arctic Ocean Seasonal Ice Zones and Implications for Pelagic-Benthic Coupling. Oceanography. https://doi.org/10.5670/oceanog.2011.74.

Wood, S.N., 2003. Thin plate regression splines. J. Royal Stat. Soc.: Ser. B 65 (1), 95–114.

Wood, S.N., 2006. Generalized additive models: an introduction with R. Chapman and Hall/CRC, Boca Raton, FL, p. 410.

Woodgate, R., Stafford, K., Prahl, F., 2015. A Synthesis of Year-Round Interdisciplinary Mooring Measurements in the Bering Strait (1990–2014) and the RUSALCA Years (2004–2011). Oceanography 28, 46–67. https://doi.org/10.5670/oceanog.2015.57.

Woodgate, R.A., 2018. Increases in the Pacific inflow to the Arctic from 1990 to 2015, and insights into seasonal trends and driving mechanisms from year-round Bering Strait mooring data. Prog. Oceanogr. 160, 124–154. https://doi.org/10.1016/j.pocean.2017.12.007.

Young, J.K., Black, B.A., Clarke, J.T., Schonberg, S.V., Dunton, K.H., 2017. Abundance, biomass and caloric content of Chukchi Sea bivalves and association with Pacific walrus (*Odobenus rosmarus divergens*) relative density and distribution in the northeastern Chukchi Sea. Deep Sea Res. Part II 144, 125–141. https://doi.org/10.1016/j.dsr2.2017.04.017.

Zhang, J., Rothrock, D.A., 2003. Modeling global sea ice with a thickness and enthalpy distribution model in generalized curvilinear coordinates. Mon. Weather Rev. 131, 845–861.

Zhang, J., Spitz, Y.H., Steele, M., Ashjian, C., Campbell, R., Berline, L., Matrai, P., 2010. Modeling the impact of declining sea ice on the Arctic marine planktonic ecosystem. J. Geophys. Res. 115, C10015. https://doi.org/10.1029/2009JC005387.

Zhang, J., Ashjian, C., Campbell, R., Hill, V., Spitz, Y.H., Steele, M., 2014. The great 2012 Arctic Ocean summer cyclone enhanced biological productivity on the shelves. J. Geophys. Res. Oceans 119, 297–312. https://doi.org/10.1002/2013JC009301.

Zhang, J., Ashjian, C., Campbell, R., Spitz, Y.H., Steele, M., Hill, V., 2015. The influence of sea ice and snow cover and nutrient availability on the formation of massive under-ice phytoplankton blooms in the Chukchi Sea. Deep Sea Res. Part II 118, 122–135. https://doi.org/10.1016/j.dsr2.2015.02.008.

Zhang, J., Steele, M., Runciman, K., Deway, S., Morison, J., Lee, C., Rainville, L., Cole, S., Krishfield, R.A., Timmermans, M.-L., Toole, J.M., 2016. The Beaufort Gyre intensification and stabilization: Amodel- observation synthesis. J. Geophys. Res. Oceans 121, 7933–7952. https://doi.org/10.1002/2014JC010158.

Zhang, J., Schweiger, A., Webster, M., Light, B., Steele, M., Ashjian, C., Campbell, R., Spitz, Y., 2018. Melt pond conditions on declining Arctic Sea Ice over 1979–2016: model development, validation, and results. J. Geophys. Res. Oceans 7983–8003. https://doi.org/10.1029/2018JC014298.